Scientific report; WR 96-06

KNMI

Microbarograph Systems for the infrasonic detection of nuclear explosions

H.W. Haak and
G.J. de Wilde

De Bilt, 1996

Scientific report = wetenschappelijk rapport; WR 96-06

De Bilt, 1996

P.O. Box 201
3730 AE De Bilt
Wilhelminalaan 10
Telefoon 030-220 69 11
telefax 030-221 04 07

Auteurs: H.W. Haak and
G.J. de Wilde

UDC: 550.348.425.4
550.834

ISSN: 0169-1651

ISBN: 90-369-2111-2

© KNMI, De Bilt. Niets uit deze uitgave mag worden verveelvoudigd en/of openbaar gemaakt worden door middel van druk, fotocopie, microfilm, of op welke wijze dan ook, zonder voorafgaande schriftelijke toestemming van het KNMI.

KNMI

Microbarograph Systems
for the infrasonic detection of nuclear explosions

by

H. W. Haak

and

G. J. de Wilde

ROYAL NETHERLANDS METEOROLOGICAL INSTITUTE
SEISMOLOGY DIVISION

August 1996

CONTENTS

Microbarograph Systems for the infrasonic detection of nuclear explosions

Abstract

This study deals with microbarograph systems for the detection of infrasonic waves. An essential part of these systems is a noise reducer, which consists of a spatial structure of pipes or hoses designed to level out the noise from small scale wind turbulence. This is achieved by spatial integration. Infrasound signals are hardly attenuated. Noise reducing structures are important for the low noise operation of infrasonic arrays.

In this study quantitative descriptions of complete microbarograph systems are given, including a theory of porous hose, which is a hose suitable for noise reducers. The relevant parameters of porous hose have been measured. Together with the details of the microbarograph itself a detailed theory is given for the design and operation of microbarograph systems.

It was found that commercially available porous hose could almost meet the criteria when smaller (around 50 meters) noise reducing systems are required. Drawbacks are the sensitivity to moist and water and the relatively small diameters available that result in high resistances. Attention is given to non-linear properties of porous hose.

The possibility of completely closed microbarograph systems is also considered. These involve noise reducers based on elasticity of the tube instead of porosity. A completely closed system is less sensitive to moist related problems. An elastic tube attenuates infrasonic waves less than porous hose. In this study the first experience is reported with an elastic noise reducer tube. We found that in practice porous hose might have strong advantages.

Microbarograph Systems for the infrasonic detection of nuclear explosions

Introduction

After a long period of diminished interest, microbarograph systems for the infrasonic detection of nuclear explosions are now under renewed study due to the ongoing efforts in the context of a Comprehensive Test Ban Treaty (CTBT). Seismology, hydroacoustics, measurements of radionuclides and the recording of infrasonic waves are the four technologies of the International Monitoring System (IMS) for the detection and identification of nuclear explosions under a future CTBT. Infrasound and the detection of radionuclides are mainly focused on explosions in the atmosphere. Only few research groups have current experience in measuring infrasound as an observatory practice.

Turbulent wind is the main source of noise in an infrasonic detection system. This conclusion is based on recent experience and is already published in the literature of the seventies (Cook, 1971), (Grover, 1971). Therefore, the construction of efficient noise reducers is still a matter of active research. An infrasonic noise reducer is a spatial structure of pipes or hoses which levels out small scale wind disturbances while leaving coherent infrasound signals of long wavelength unaffected. The noise reducer is based on spatial filtering and not on a frequency filter, since the frequency content of signal and noise is comparable. The frequency range of interest is 0.001 - 20 Hz.

In the literature on infrasound a variety of terminology is used to describe essentially the same measuring equipment for the detection of infrasonic waves, such as low frequency microphones, microbarographs, microbarometers and infrasonic detectors. The noise reducers are also known as Daniels tubes, line microphones, pipe arrays, pipe filters or space filters.

Array considerations

Microbarograph systems are usually operated in small arrays (Haak, 1996). The base line of four element arrays, as proposed in the IMS, is chosen between 1 and 10 kilometers depending on local conditions such as the wind noise. Usually an equilateral triangular configuration with one centre element is chosen. Square configurations are also a viable alternative. Should one of the elements be disfunctional, the remaining configurations of a square array are more satisfactory than those of a triangular array (see appendix III).

For proper array operation it is required that the amplitude and phase response functions are equal among the individual sensors. This demand requires that the sensors are physically identical and that the site conditions such as temperature and humidity are comparable for the array. Noise reducers and microbarographs form one system in this respect, in which both parts contribute to the response.

Recent developments

Compared to the late sixties and the early seventies, when the infrasound technique was developed, it is now relatively easy to set up a proper infrasound monitoring system. The advances in computing and electronics make it easy to use off-the-shelf equipment and software for detection, array processing, data storage and high resolution A/D-conversion. From the related field of seismology a lot can be learned in this respect. The synergy between the two monitoring techniques, however, can only be partly extended to the development of infrasound detectors. The same applies to the mechanics of noise generation. In this study, therefore, we focus on the detector and in a later study we intend to focus on wind as the main generator of infrasonic noise.

Microbarographs

Infrasound of natural origin has an acoustic pressure in the range of 0.1-100 dyn/cm^2. Various pressure units exist: 1 dyn/cm^2 = 1 μbar = 0.1 pascal (Pa). The atmospheric pressure is about 10^6 dyn/cm^2 = 10^5 Pa = 1000 hPa = 1000 mbar, with natural pressure fluctuations of 20%. The broad band frequency range of interest is 0.001- 20 Hz or somewhat more narrowed down to 0.01- 5 Hz. The influence of wind speed v is essentially given by the law of Bernoulli:

$$p + \frac{\rho v^2}{2} = constant \; ; \qquad \Delta p \approx \rho v \Delta v \tag{1}$$

The second part of (1) represents pressure fluctuations as a result of wind speed variations. Variations in wind speed Δv of 4 m/s at a wind speed v of 8 m/s result in pressure variations of 40 Pa. These signal and noise figures will determine the design of microbarographs with respect to sensitivity and dynamic range.

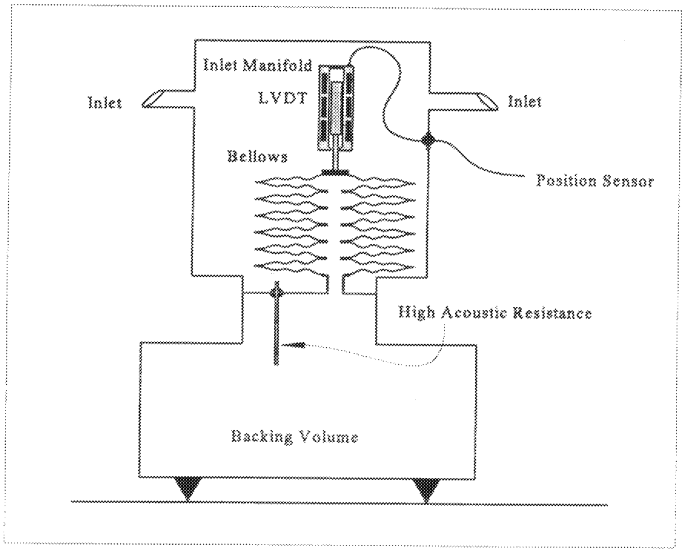

Figure 1.
Schematic overview of a differential pressure microbarograph.

The differential pressure microbarograph produces an electrical signal proportional to the difference between the ambient pressure at the input volume and the pressure in a backing or reference volume (figure 1). A small air leak between the two volumes will lead to a pressure equalisation over long periods of time. This determines the low frequency response of the system. The effect is that the long period pressure fluctuations which are usually substantially larger then the acoustic pressures, are effectively suppressed. The pressure sensing component is a bellows. The differences in pressure between inlet and backing volume for periods of the order of 1000 seconds are usually small, so the measuring bellows can be made quite sensitive to small pressure differences.

The position of the bellows' top is transformed to an electrical signal with a position sensor such as a Linear Variable Differential Transformer (LVDT) or a capacitance sensor. Both are in principle readily available low noise devices. Since the pressure forces on the bellows are substantive, no special care is needed to diminish forces between the transducer and the sensing element.

The instrument described above has the disadvantage of being sensitive to temperature gradients between the two volumes. It is therefore good practice to locate the entire unit a few meters below the surface to make use of the enhanced temperature stability at some depth. In order to reduce the pressure noise even further the backing volume can be filled with steel wool or vermiculite (Cook, 1971). The temperature dependence in numerical terms amounts to 3.4 mbar/ ^{0}C = 340 Pa/ ^{0}C, based on the ideal gas law: $dP/dT = P/V$. For comparison: the height gradient of the atmospheric pressure is 12 Pa/m.

A way to overcome this problem is to use a vacuum bellows as a primary sensing component. This can be fitted with or without a spring inside to counteract the large external pressure. At a moderate vacuum of 10^{-3} Torr (0.13 Pa) the temperature dependence is reduced to 0.45 mPa/ ^{0}C, which is quite acceptable, considering the noise and signal levels (figure 2).

The consequence of this choice is that the microbaragraph is turned into an instrument for the measurement of absolute pressure. The need for the backing volume has disappeared. Now, the only drawback is the large dynamic pressure range due to slow atmospheric pressure changes. This exceeds 200 hPa. Fortunately, readily available high resolution 24-bits A/D-converters and electronic filtering will adequately solve this problem. In the absolute instrument the temperature dependence of the bellows' spring becomes important. The best designs use materials for the construction of the bellows and spring that are hardly influenced by temperature changes on elastic constants. Furthermore, the relatively large movements of the bellows' head will need care, with respect to signal induced noise.

A particular problem with both instruments is the mechanical resonance of the bellows as a mass-spring system. The transverse oscillations have the lowest frequency. These are easily removed from the frequency band of interest towards higher frequencies with a spider spring attached to the top of the bellows. The longitudinal oscillations should also be in a frequency range above the relevant band width of the instrument. This, however, will limit the sensitivity of the bellows. Feedback systems will be a solution for both dynamic range and resonance problems, especially in broad band sensors.

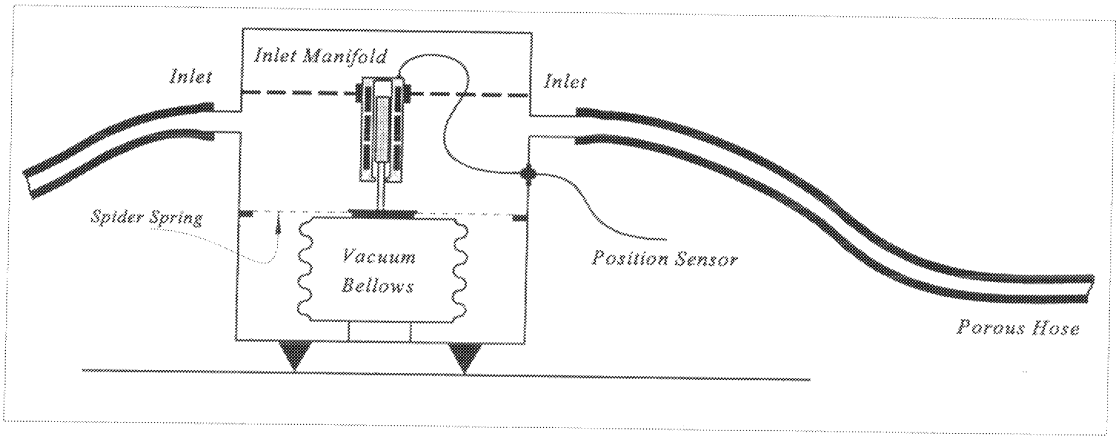

Figure 2.
Schematic overview of an absolute pressure microbarograph.

The two types of microbarographs described above are examples of pressure sensing instruments which use bellows as the primary sensor. They belong to the most rugged and well established pressure sensing devices. Many other pressure measuring devices are described, based on various principles such as temperature change of a hot wire due to air flow or frequency change of a piezoelectric crystal upon atmospheric pressure. None of those techniques will be able to control each step in measuring to the same degree as simple bellows and position sensors can. Both instruments have, however, rather large volumes. The loading of the noise reducing structures can be a drawback since the pressures in the instruments will be lower. The theory is given in appendix I.

Little attention has been given to the possibility to use a magnet coil velocity transducer as a detector for the movement of the bellows head. Such a transducer, however, is robust, is very low noise and gives the instrument a response in accordance with wind noise characteristics. The integration to pressure can be done digitally.

Electret microphones

Electret microphones are not generally used in infrasound detection. The frequency response of these very sensitive and low price devices extends to periods between 50 and 100 seconds. A drawback is their variability in low frequency amplitude response and their sensitivity to moisture. When multiwire cables are used the electret microphone can be utilized to build rather efficient noise reducers. By simply summing the output signals from each individual electret along a cable in a circle or a straight line the air pressure variations can be averaged over an extended area.

Another distinct application of electrets is the study of noise reducing structures themselves, since the electret microphones are small (~ 5 mm) and can be inserted into the noise reducer pipes. In this way amplitude, phase and propagation velocity can be measured in situ.

Noise reducers

An infrasonic noise reducer is a spatial structure of pipes or hoses attached to the input of the microbarograph to level out small scale wind disturbances while leaving coherent infrasound signals of long wavelength unaffected. The noise reducer is based on spatial sampling and filtering and not on a frequency filter, since the frequency content of signal and noise is comparable. The purpose of a noise reducer is to sample an area larger than the turbulence scale of the wind. At the same time, the dimensions of the noise reducer should be smaller than the characteristic wavelengths of acoustic waves under consideration.

To distribute the input over a wide area, a network of acoustic wave guides can be used. Daniels (1959), for instance, proposed a line microphone; a tapered pipe that is coupled to the atmosphere by means of a series of acoustical resistances at equal intervals along the length of the pipe. The tapering was introduced to achieve constant impedance along the line. Later Burridge (1971) gave a theoretical description of a less complicated noise reducing system that was made of a ring of narrow tubing of uniform bore (see appendix X). The inlet ports were again equidistant capillaries. Grover (1971) tested such a system with good results.

In recent years noise reducing structures were tested that made use of porous hose in circle or star configurations (see figure 3). Porous hose or soaker hose is used in gardening to wet the soil. In the infrasound application it constitutes a distributed inlet port just as the other properties of the wave guide are distributed. In figure 3 the first 10 meter of hose is standard fully closed garden hose in order to avoid sampling too densely in the vicinity of the microbarograph. This also reduces moist problems in the central microbarograph.

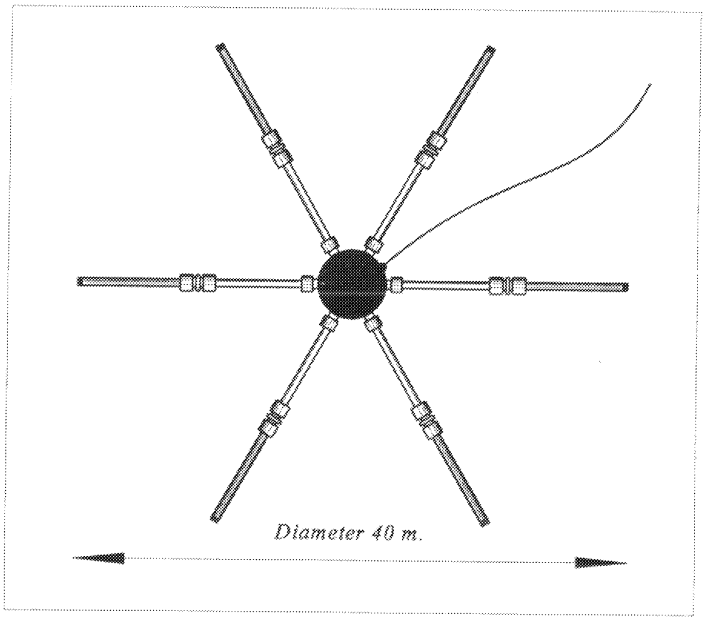

Figure 3.
Schematic layout of a six-arm noise reducer. The individual components are not drawn to scale.

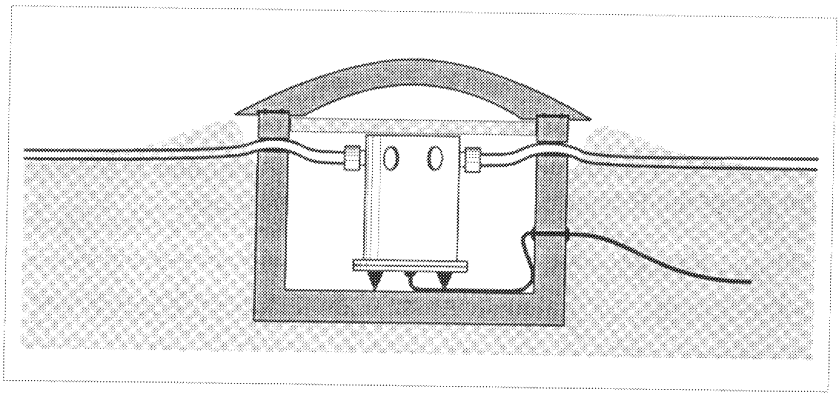

Figure 4.
Field impression of a microbarograph shelter. The streamlined roof of the shelter has a styrofoam temperature shield.

Figure 4 gives an impression of a microbarograph system in the field. In order to ensure stable operation under a variety of climates with a minimum of maintenance, great care should be taken with respect to the housing of the equipment. Under the mild condition of the Netherlands a concrete structure as in figure 4 has given good results. By burying the system, including power cables and data transmission lines, temperature stability is gained and the system is more or less tamper proof.

Some problems may occur. One problem is the influence of moist, water and ice, especially in the porous hose noise reducing structure. Dirt may clog the micropores when the porous hose is left unattended on the ground over an extended period of time. Two combined and partial solutions are proposed by a French research group (LDG): covering the hose with a small roof and lift the hose slightly (< 1 m) from the surface. See also appendix IX. Although the increased wind velocities higher above the surface and the fact that in general the use of larger windshields is not favourable (Grover, 1971), the influence of a small curved roof might be small. A completely closed system, however, would be preferable.

An other problem occurs when the housing of the equipment changes the wind patterns resulting in excess noise when it is made too large. Therefore a streamlined low roof of the instrument shelter (figure 4) and a grass surface for the noise reducer area are recommended.

In general the field set-up of the instruments is an important subject where good guidance is needed, since experience over extended periods of time and in different climates is of importance. Only a combined effort can lead to optimal solutions, both locally and globally.

To improve the overall coverage of an area, curled and branched patterns of noise reducer hose can be tested. This will only produce good results when the total length of the (porous) hose is shorter than the characteristic attenuation length. In the case of branching, impedance matching is needed at each fork.

Theory of noise reducers

A basic priciple of the theory of noise reducers is the notion that the structure of hoses or pipes are wave guides or transmission lines with a characteristic impedance and propagation constant. Theory assumes that the flow in the noise reducers is laminar, not turbulent. In general this condition is fulfilled when the Reynolds number is not exceeding values of 2300. For straight pipes the Reynolds number *Rey* is defined as:

$$Rey = \frac{d v_{av}}{\nu} = \frac{d v_{av} \rho}{\eta} = \frac{4 f_v}{\pi d} \frac{\rho}{\eta} \qquad (2)$$

in which d is the pipe diameter, v_{av} the average air velocity, ρ the density, η the dynamic viscosity, ν the kinematic viscosity and f_v the volume velocity. The critical velocity in m/s is $2.9/d$ by rule of thumb, with the tube diameter d in cm (Ower et al., 1977 p. 77). Given the acoustic and wind pressures and the characteristic pipe dimensions the flow type is usually laminar in noise reducers. Only exceptional circumstances, such as a 100 Pa pressure over a tube with 1 cm^2 cross-section and with an acoustic resistance of one acoustic ohm, will lead to velocities of 10 m/s.

The acoustic transmission line is characterized by the specific impedance Z and the propagation constant Γ, Z_0 is the lossless impedance :

$$Z = \sqrt{\frac{R + i\omega L}{G + i\omega C}} \qquad \Gamma = \sqrt{(R + i\omega L)(G + i\omega C)} \qquad Z_0 = \sqrt{\frac{L}{C}} \qquad (3)$$

For low frequencies R corresponds to the resistance due to viscous losses. L is the acoustic inertance, which corresponds to the effective mass of air taking part in the vibration. G is the acoustic conductance and is due to heat conduction (Daniels, 1950). In the case of a porous hose it is also due to the leak. C is the acoustic compliance, it corresponds to the reciprocal of the stiffness of air. The analogue with electrical transmission lines is often used in complex acoustic systems for pragmatic reasons. In figures 5a and 5b an acoustic and electronic diagram is given of a short transmission line section.

Benade (1968) calculated all the relevant parameters R, L, G and C as a function of tube radius and frequency, describing a non-porous hose. In a simple experiment suggested by Grover (1971) for the measurement of acoustic resistances of capillaries, we determined the acoustic resistance $1/G$ resulting from the porosity of the soaker hose. This is described in detail in appendix II. Now, all the relevant parameters of the various hoses are known.

The one dimensional propagation of acoustic pressure waves in both directions through the tube approximated as propagation through an acoustic transmission line is given by:

$$p(x,t) = (A e^{-\Gamma x} + B e^{\Gamma x}) e^{i\omega t} = A e^{i(\omega t - kx)} e^{-\alpha x} + B e^{i(\omega t + kx)} e^{\alpha x} \qquad (4)$$

If Γ is written as a general complex number $\Gamma = \alpha + i\beta$, then β is the wave number and α is the attenuation constant. In this way the phase and group velocities can be calculated. This gives a full characterization of the infinite transmission line without termination impedance.

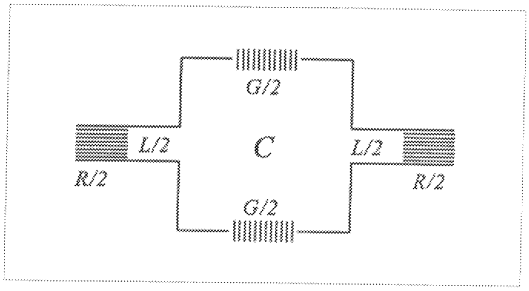

Figure 5a.
Schematic diagram of an acoustic wave guide.

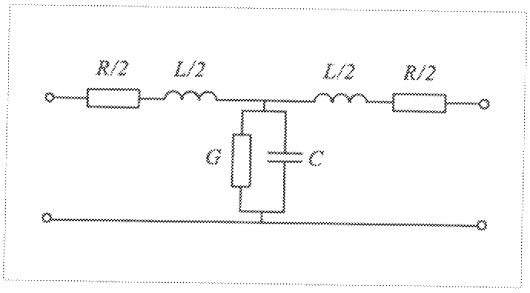

Figure 5b.
Electronic analogue of an acoustic wave guide.

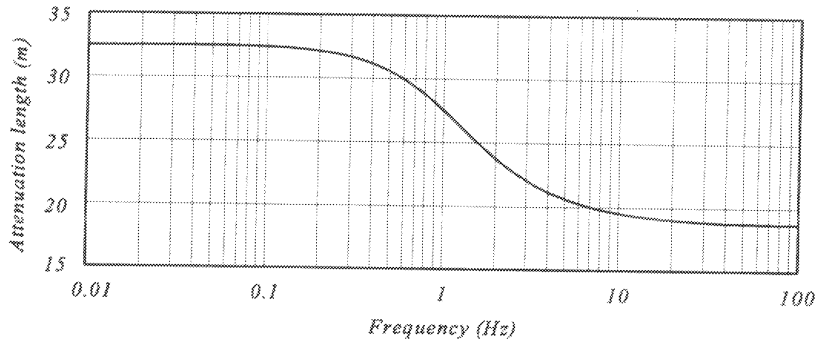

Figure 6.
Attenuation length as a function of frequency for a porous hose of 12 mm inside diameter.

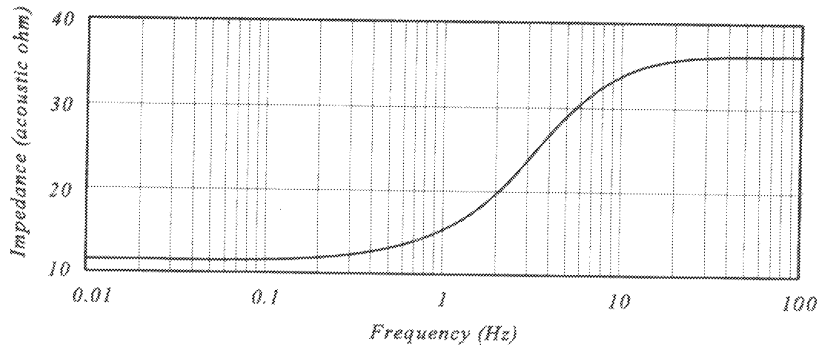

Figure 7.
Impedance in dyn cm^{-5} s as a function of frequency for a porous hose of 12 mm inside diameter.

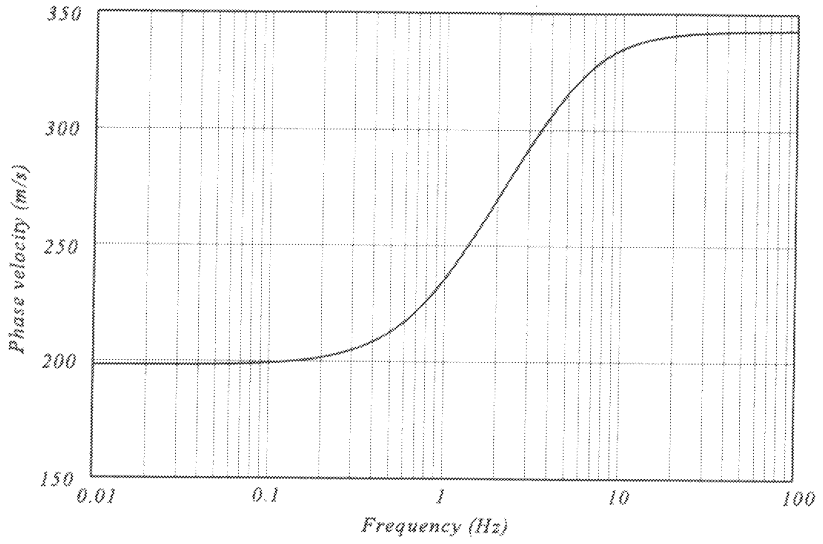

Figure 8.
Phase velocity versus frequency for a porous hose, inside diameter 12 mm .

As can be seen from figures 6,7 and 8, the characteristics of the tube change when the frequency exceeds approximately 1.0 Hz. This frequency can be altered by adjusting R, L, G and C. In a distortionless line the parameters are adjusted according to $R/L = G/C$ or $RC = LG$. Such a distortionless line has the property of leaving the shape of the signal unchanged during propagation although attenuation of the amplitude of the signal exists. The purely resistive impedance a distortionless line is equal to that of a lossless line and is given by Z_0. This makes proper termination with a capillary easy.

The currently used porous hose can be made into a distortionless line by reducing the porosity with a factor ten. The attenuation length will increase to circa 100 meter. This can be the solution for larger noise reducing structures, although standing waves are more prominent at frequencies above 1.0 Hz. The reduction of porosity can be achieved by partially blocking the micropores with paint.

A distortionless line has no change in impedance, phase velocity and group velocity as a function of frequency. There is, however, a change in the propagation constant of the tube. Only the imaginary part, the wave number, changes with frequency. The use of such lines should be seriously contemplated for larger broadband noise reducer systems that can be built from engineered tube materials.

To construct a complete microbarograph system several branches of noise reducer tubing are connected to a central microbarograph. The volume of the microbarograph is loading the noise reducing transmission lines; on the other end the line is closed. The total response of the system can be calculated. To do so Burridge (1971) assumed a signal present at only one inlet port of the noise reducer (see appendix VI). The response of the complete microbarograph system to this stimulus represents a measure for the suppression of a localized gust of wind.

Several conclusions can be drawn from the theoretical results. First, the volume of the microbarograph itself has a strong effect on the response of the noise reducer for frequencies above 0.5 Hz. This effect also depends on the length of the noise reducing structure; here lengths of 20 m and longer were assumed.

Secondly, the practical length of noise reducer tubes is a direct function of the porosity of the tube since this parameter determines the decay length of the propagating waves. Tubes shorter than the decay length will not sample an area large enough, and when the tubes are made substantially longer, the signal will not reach the microbarograph detector. Circular noise reducers are not better than star configurations. For details see appendix X. The lowest mode has a wavelength equal to the perimeter of the ring. For star configurations the lowest mode equals the radius.

Thirdly, the value of the porosity of commercially available hose makes the noise reducing structure more sensitive to the microbarograph detector with smaller distances. Therefore as is illustrated in figure 3, a system can be designed that uses a combination of both porous hose and standard closed hose for a better distribution of sensitivity. In our system the crude approximation is made by using 10 m of closed hose near the detector connected to 10 m of porous hose. This system works fine in practice, provided the readily available tube fittings and connectors from the gardening industry.

Although it is quite easy to use standard porous hose, the question is whether this type of hose, which is more or less by accident suitable for our purposes, is really the best possible choice. The current applications are limited to distances of approximately 50 meter. The porosity of the hose depends on the humidity. The resistance increases from 380 acoustic ohm meters in a dry situation to 620 ohm meters and higher in a moderately wet environment. During the numerical evaluation of various tube parameters it was noted that especially the diameter of the hose played a crucial role in the attenuation of the noise reducer. A larger diameter, e.g. 50 mm instead of the standard 12 mm, will increase the attenuation length from 30 to 400 meters.

Closed system noise reducers

From a purely practical point of view porous hose still suffers from being sensitive to water and moist especially when lying on the ground. Apart from having non-linear input resistances, porous hose also has a resistance depending on the weather situation. This prompted us to consider a closed tube system. Such a system has the advantage of leaving the microbarograph itself completely dry, preventing corrosion in the long term at sites near oceans. It should be remembered, however, that a high acoustic resistance might be needed to level the slowly fluctuating static pressure in order to avoid excessive elastic strains on the tubes. On the other hand noise reducer systems are possible where the inside pressure differs from the ambient pressure to keep the tube in shape in order to have a fixed elastic response.

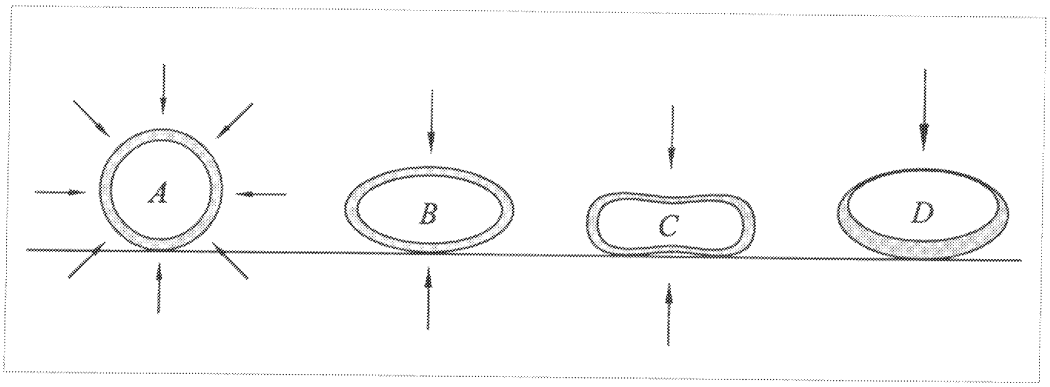

Figure 9.
Cross-sections of various types of closed hose with increasing sensitivity for external pressure changes from A to D. C can operated with underpressure, B and D with overpressure.

In figure 9 the basic shapes are illustrated of such hoses. The idea is that the elasticity of the hose is used instead of the porosity to transmit pressure changes inside the tube. Now it is no longer the flow of air into a cylindrical conduit but the elastic response of the hose itself that transmits the signal. Of course, the wave guide action of the tube is retained. So far we found that soft silicone tubing works best, also at low temperatures. At -20 °C silicone tube still has fairly elastic properties. The optimum solution would be if silicone hose could be manufactured with oval cross-sections (B through D in figure 9) to enhance the sensitivity and with elasticity constants that are not sensitive to temperature changes. Preliminary experiments with oval shaped silicone tube of 12 to 20 mm inside diameter and with a wall thickness of 1 to 3 mm show promising results. The configuration of figure 3 is used with six arms. A concern is the response to temperature fluctuations in the pass band of the instrument. Various climates may need different solutions. This also applies to the black coloured porous hose. An alternative may be the use of fluid filled tubes, which have the additional advantage of having high phase velocity for compressional waves. In figure 10 some more examples are given of tubes, which are of composite structure. In appendix VIII the theory is presented of wave propagation in a closed elastic hose.

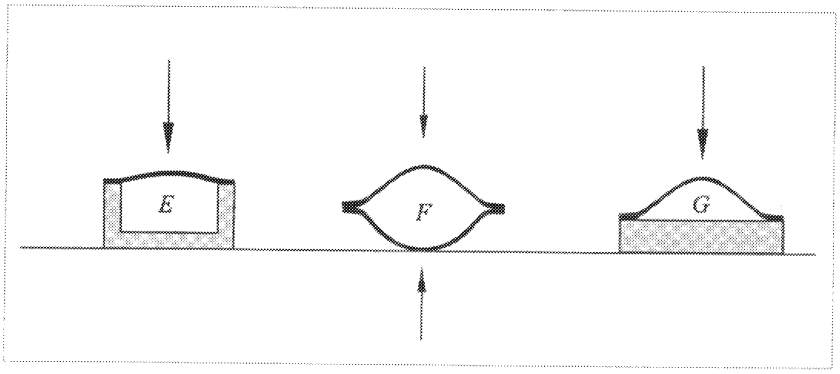

Figure 10.
Cross-sections of various types of closed flexible structures.

Response to noise of a microbarograph system

When the impedances of both the microbarograph and the hose are known, the total response of the system to both signals and small scale wind turbulence can be calculated. In order to avoid confusion with the response of the microbarograph itself, the absolute microbarograph is chosen in this section as a reference even, without an inlet tube which is in accordance to the real situation. In essence the response of the six-arm star configuration is that of one noise reducer arm loaded by a combination of the microbarograph volume and the impedance of the other five porous tubes. In appendix VI a short theory is given. In figure 11 two noise reducer configurations are illustrated, which are used in the calculations.

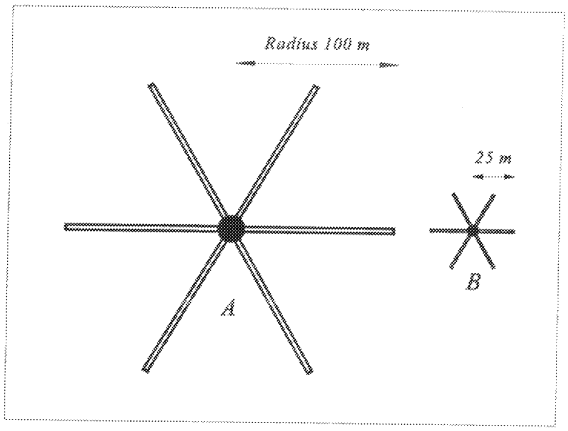

Figure 11.
Overview of two six-arm star arrays.
Both arrays use porous hose only.

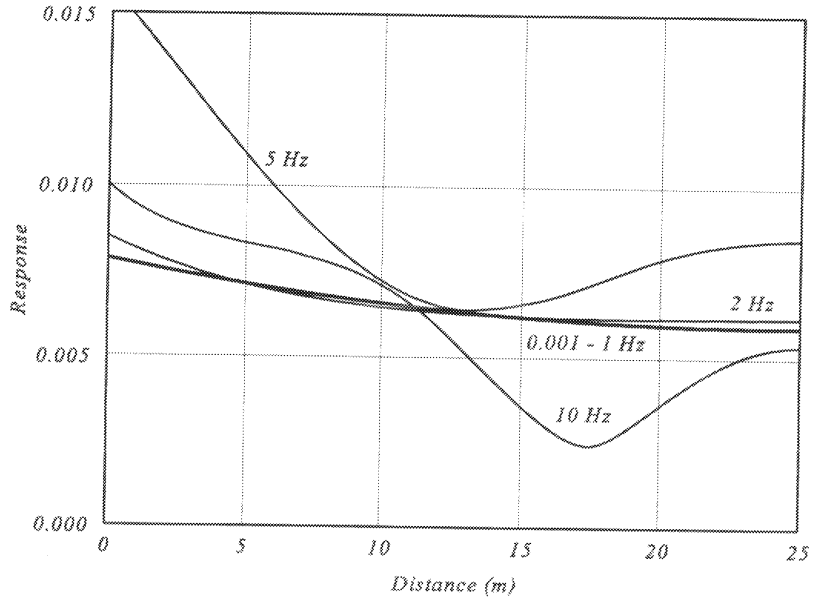

Figure 12.
Absolute value of the response of a microbarograph system including noise reducer to a 1.0 Pa harmonic pressure over a length of 1.0 m of 12 mm diameter porous hose as a function of the distance to the microbarograph.

In figure 12 the noise response is given as a function of distance of the localized pressure disturbance from the central microbarograph. The actual numbers correspond to the ratio of pressures inside the volume of 3.8 liters of the microbarograph and the input pressure over a length of one meter of the porous hose. In this example the porous hose has a length of 25 m.

From figure 12 it is clear that there is a slight decrease in sensitivity toward longer distances from the central microbarograph. This dependence will disappear when the radius of the tubing is larger than 12 mm. Also, it is clear that between 1 Hz and 10 Hz the response is more variable. In this frequency range also large phase changes to the signal occur. In appendix VI a theory is given equivalent to that of Burridge (1971) used to calculate this figure. This theory produces results identical to that of Burridge when the same systems are considered. The theory in appendix VI also describes systems with continues inlets.

When porous hose with a larger tube diameter is used, larger noise reducing structures can also be built. The porosity of the hose could then be adjusted accordingly. For instance an increase to a tube diameter of 50 mm under the condition of the same porosity per meter will make the response almost flat as a function of distance to the barograph. For low frequencies the attenuation depends on the product of R and G (see equation 3). So both parameters can be changed in order to get the desired attenuation. At high frequency strong oscillations in sensitivity will occur due to the generation of standing waves in the system.

In figures 13 and 14 the response of such a wider tube system is illustrated. Above 1 Hz the strong oscillations are clearly visible (figure 14). The pattern of the oscillations corresponds to the pattern of pressure of the standing wave as if the source was situated at the detector in the centre. It is an example of the reciprocity principle. The system is therefore most sensitive to the outside pressure in the antinodes with high impedance and least sensitive in the nodes with low impedance of this oscillation mode.

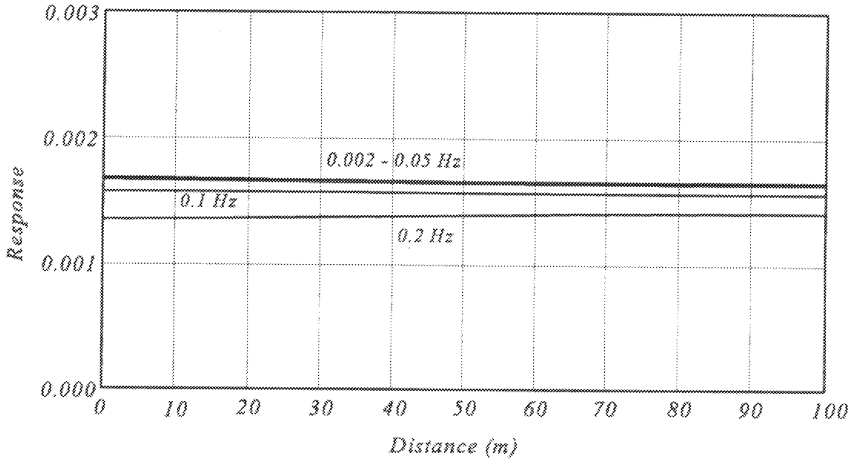

Figure 13.
Absolute value of the response for low frequencies of a microbarograph system including noise reducer to a 1.0 Pa harmonic pressure over 1.0 m of 50 mm diameter porous hose as a function of the distance to the microbarograph.

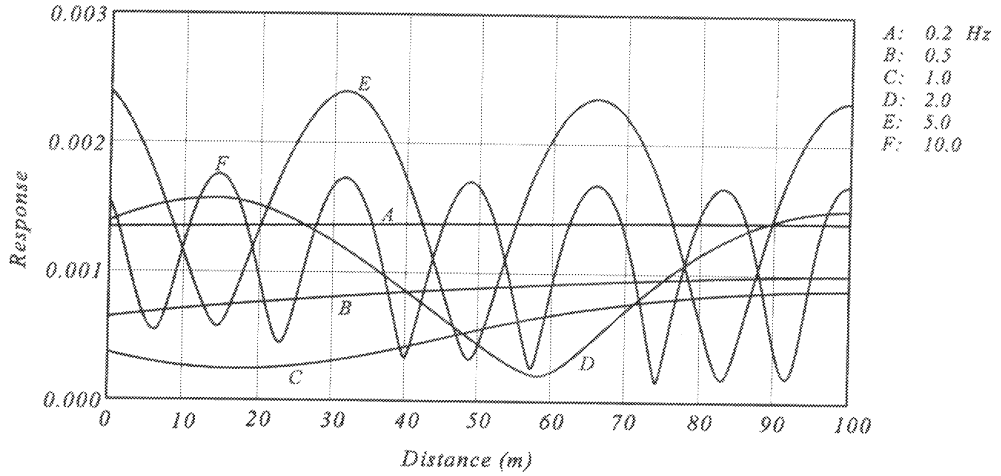

Figure 14.
Absolute value of the response for high frequencies of a microbarograph system including noise reducer to a 1.0 Pa harmonic pressure over 1.0 m of 50 mm diameter porous hose as a function of the distance to the microbarograph.

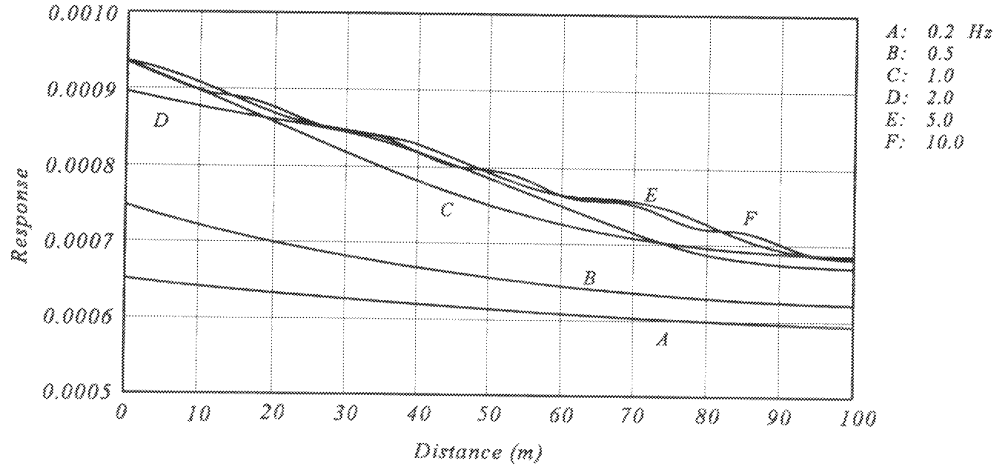

Figure 15.
Absolute value of the response for high frequencies of a microbarograph system to a 1.0 Pa harmonic pressure over 1.0 m of 50 mm diameter porous hose as a function of the distance to the microbarograph. The end points of the noise reducer tubes are terminated with a pure resistive element with a value of Z_0. Frequencies lower than 0.2 Hz behave like curve A.

The strong oscillations at high frequencies hinder broad band operation of the microbarograph system. It was found that proper termination of the noise reducer tube at the extremities and even at the microbarometer inlet is essential to avoid such oscillations. As was made clear in figure 7 the impedance is frequency dependent. Consequently the terminator should follow the same frequency dependence. A terminator may in practice be hard to realize. From calculations it becomes clear that terminating with an acoustic resistor with a value of the characteristic lossless impedance Z_0 as defined in equation (3), will reduce the oscillations to a large extent (figure 15). The terminator puts a dissipative load on the system, therefore the pressure reduction is larger for noise and signals. The terminator can be a simple small tube or capillary of the right diameter and length. The value of Z_0 is usually lower than the value of the inlets. Therefore, the terminator could influence the intake of the signals when it is left open to the outside atmosphere. A solution to this problem is to surround the terminating resistance with a volume. In turn the volume will influence the terminating impedance for low frequencies were interference is not a problem. The simplest solution of the whole termination problem is to use a tube far longer than the attenuation length.

With the above considerations all elements are available for the design of a proper noise reducer. In order to have a smooth impedance as a function of frequency, the starting point is a distortionless line. This condition results in the value for the input conductivity G being more or less fixed and independent of the tube diameter. This can be understood in the following way. L/C is mainly dependent on the elastic properties of air and on the tube diameter d, it is proportional to $1/d^4$. In a distortionless line R/C is fixed. If Poseuille type viscous flow is assumed, R is also proportional to $1/d^4$. It follows that G is independent of the tube diameter in a distortionless line, with $L/C = R/G$. The real part of the propagation constant e.g. the attenuation constant α of equation (4) is given by R/Z_0. In good approximation the attenuation is a function of the tube diameter only in a distortionless line.

First, the arm length of the array should be selected, e.g. 100 m in figure 15. Then the accepteble change in sensitivity along the arm is chosen, e.g. 10 - 20%, depending somewhat on the frequency. Then the resistance R can be calculated from the known attenuation constant. Using the known resistance R, the diameter of the tube can be found. In figure 15 the diameter of the tube is 50 mm.

When the noise reducer tube branches into two tubes of the same diameter, proper termination can be achieved by a resistive element in each branch with a value of $1/3\ Z_0$ (see figure 16). When in total N branches come together in one point the resistive element has a value of $(N-2)/N\ Z_0$. This is also the solution to terminate the six hoses properly at the inlet of the microbarograph, provided its volume is small.

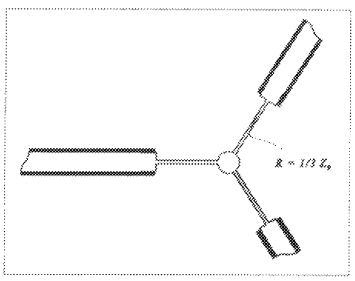

Figure 16.
Reflection free termination of a branch.

With proper termination the objective that only pressure waves towards the microbarograph should occur can be achieved. This was also Daniels' design goal when he designed his line microphone (Daniels, 1959). The conclusions above are also valuable in the case of a discrete inlet port noise reducer with uses capillaries instead of porosity as long as the system can be approximated as a distributed inlet system, i.e. with small separations between the inlets. This is usually the case. In a second phase of this study an experimental verification under field conditions is proposed.

Response to signals of a microbarograph system

When the response of the system is considered with respect to propagating signals, it should be realized that for most low frequencies the wavelengths are larger than the noise reducer dimensions. In this case the noise reducer and barograph can be lumped together in a discrete component system. In figure 17 the symbolic analogues are given both in acoustic and in electronic terms.

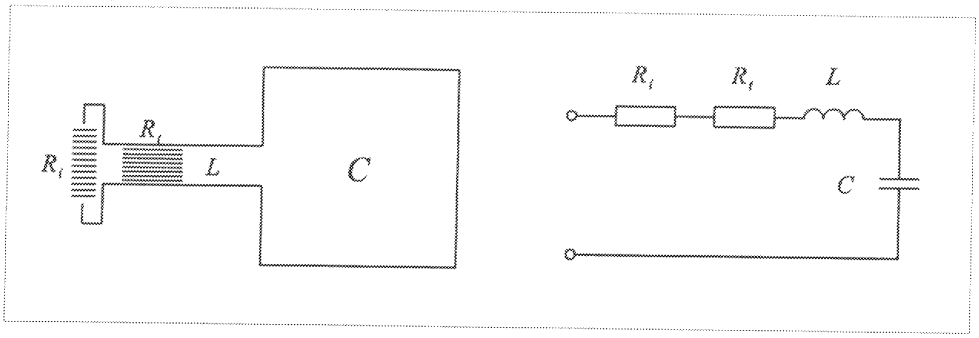

Figure 17.
Acoustic scheme and electronic analogue of a complete microbarograph system at low frequency.

The response is 1.0 with the measured values for the total input resistance R_t of the porous hose, the tube resistance R_t , the tube inertance (inductance) L and the compliance (capacitance) C of the volume of the microbarograph. For low frequencies the input pressure is therefore equal to the pressure inside the microbarograph we have tested, as in figure 3.

For higher frequencies or for wavelenghts comparable with the dimensions of the noise reducer, a different approach is taken. First it should be realized that the response of the microbarograph due to a point source of 1.0 Pa applied along the arms of the noise reducer as a function of distance $\Delta(x, \omega)$ is the same as the pressure ratio that would occur if a source of 1.0 Pa is situated at the microbarograph and the pressure just outside the tube is followed. This is known as the reciprocity principle between source and receiver. The theory is dicussed in appendix VI; figures 12 - 15 illustrate $\Delta(x, \omega)$.

The reciprocity principle can be taken one step further. If the response is needed from plane incoming acoustic waves, then a calculation of plane waves resulting from a source at the central microbarograph gives the same answer. In terms of an array, the arms of the noise reducer are treated as continuous array elements. In the case of discrete inlet ports the inlets are treated directly as array elements. The response function A of the microbarograph and noise reducer is given by:

$$A(\omega,\vec{p}) = \int_{nr} \Delta(\omega,\vec{r})\, e^{i\omega\vec{p}\cdot\vec{r}}\, d\vec{r} \qquad with \qquad \vec{p} = \frac{\hat{l}}{c} \tag{5}$$

The integral is taken over the porous hose section of the noise reducer (nr), c is the sound velocity in air, p is the slowness vector. Figure 18 illustrates the response function $|A|$ for a six-arm noise reducer system with a radius of 25 m at a frequency of 5 Hz. The arms were terminated with a high impedance. At frequencies lower than 5 Hz the response is almost independent of azimuth. The amplitude of the response function is near unity. Figure 18 also shows that the sensitivity at higher slowness, or lower apparent velocity, is rapidly decreasing. This effect is stronger at higher frequencies. Here the function of the noise reducer as a spatial filter or a slowness filter becomes clear. A strong wind of 20 m/s has a slowness as high as 50 s/km and falls outside the range of this figure.

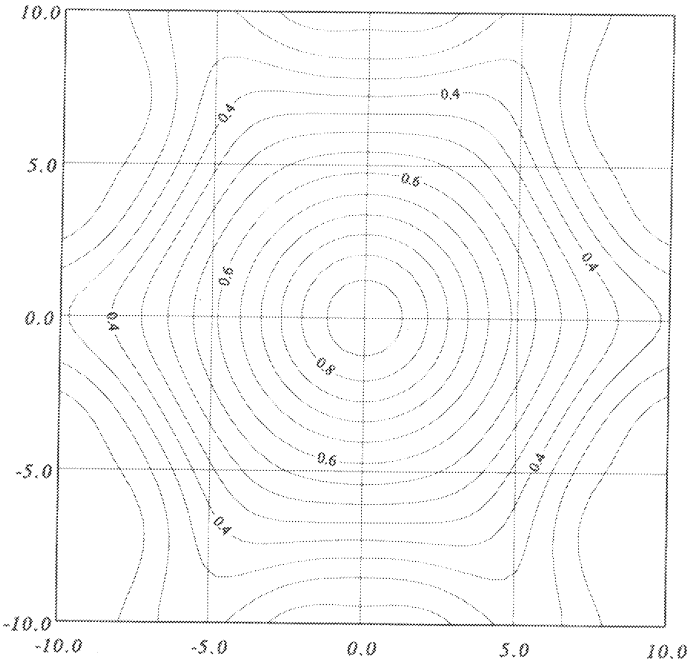

Figure 18.
Power of the response function of a six-arm noise reducer system with a radius of 25 m at a frequency of 5 Hz. The horizontal and vertical axes are the two components of horizontal slowness in s/km. The orientation of the arms is the same as in figure 11.

Adiabatic to isothermal transition

It has been known since the determination of the sound velocity in air that sound in free space behaves as an adiabatic process: this means without exchange of heat with the surrounding medium. In sound propagation the wavelength scales with oscillation period, therefore in free air sound is adiabatic. This assumption is no longer valid if pressure wave propagation is studied in narrow tubes or volumes where heat conduction effects may not be neglected. In this case a transition to isothermal behaviour can be observed.

A full description of noise reducers tube is given by Benade (1968). He describes sound propagation in tubes with an "exact" theory, with viscous effects depending on volume velocities and with kinetic energies, that correspond to resistive effects (R). He also describes thermal energy losses that are due to failure of adiabaticity at the walls, associated with the potential energy of compression. These correspond to conductive effects (G).

In fact there are two more or less independent processes: a thermal process and a viscous process. Each of these processes involve boundary layers. The two processes originate from the same root, according to the kinetic gas theory. Both processes are connected by the mean free path of air at ambient temperature and pressure. Viscosity and thermal conductivity are both proportional to the mean free path. The two boundary layers are numerically only slightly different. For viscosity there is a transition from the Poiseuille description at low frequencies and small tube diameters to the Helmholz-Stokes description at high frequencies and large tubes (appendix IV). The Poiseuille description is associated with the isothermal regime and the Helmholz-Stokes description is connected with the adiabatic regime.

The analytical approach of Benade is valuable but can only be applied to systems with simple geometry. When studying more complicated systems are to be studied, such as a microbarograph of complex geometry, an experimental approach is more suitable to obtain the relevant parameters.

Within the pass band of the infrasound system both the noise reducer and the microbarograph have a transition to isothermal behaviour. As explained above an experimental solution has to be found for the microbarograph. Appendix VII describes the classic experiment of Clement and Desormes, which measures the time scale of this fundamental phenomenon. Of course, the two transition frequencies between adiabatic and isothermal need not be the same for the noise reducer and the microbarograph. The results are of importance for proper design and calibration of microbarograph systems.

The experimental results indicate that for a microbarograph of regular size, time constants are involved of the order of seconds. This depends on the size and the filling of the instrument. In a microbarograph with a volume of 3.5 litre a time constant was measured of 4.2 seconds with the method using a volume change of 50 ml. This time constant corresponds to a frequency of 0.04 Hz. For non-porous tube of 12-20 mm diameter it was calculated that the transition occurs between 0.1 and 1.0 Hz. Larger tube diameters result in lower frequencies for the transitions. This effect shapes the frequency response of the microbarograph system.

Conclusions

Microbarograph systems for detection of infrasonic signals generally consist of a pressure detector, the microbarograph itself and a noise reducer. With respect to the microbarograph detector a variety of instrumental solutions exist that will meet the specifications. Careful design of a microbarograph should not only include the classic parameters such as low instrumental and electronic noise, good high frequency response and temperature stability, but should also be guided by the connection to the noise reducing structure. This involves the complex input resistance of the microbarograph.

Noise reducers are not as thoroughly investigated. Today it is still hard to find a noise reducer that is easy to construct, that is robust in various environments and that is low priced. In this paper much attention is given to porous hose as a good noise reducing tube that could meet the above criteria. We measured that commercially available porous hose had an acoustical resistance of 380 cgs acoustic ohm for a length of one meter. Together with already known values from the literature for other parameters, this value was used for a theoretical description of a complete microbarograph system. Porous hose of this type could almost meet the criteria when smaller (circa 50 meters) noise reducing systems are required. Drawbacks are the sensitivity to moisture and water and the relatively small diameters available that result in small attenuation lengths.

Completely closed noise reducers are under development, possibly with favourable robustness and lower in price. These systems still have to be tested under various environmental conditions.

A microbarograph system should be regarded as a whole: noise reducer and pressure detector are integral parts of a complete measurement system. In broad band applications it is important to realise that the high frequency part of the spectrum deserves special attention because here the volume of the detector and the noise reducing structures are interacting, resulting in a strong influence on the response. A true broadband system, in the frequency range of 0.001 - 20 Hz is very well possible given proper termination of the noise reducer.

Theoretical considerations of this type are important in the design and the calibration phase of instrumental development, since true field tests and calibration of these instruments is tedious and time consuming.

Appendix I *Theory of the absolute microbarograph*

The theory of the differential pressure microbarograph is given by Burridge (1971). The theory of the absolute instrument given here uses a comparable method and notation. Starting with the application of Boyle's Law to the gas inside the microbarograph with volume V and with ambient pressure P_A, the following general expression is obtained after logarithmic differentiation with respect to time:

$$P_A V = constant \quad ; \quad \frac{\dot{P}}{P_A} + \frac{\dot{V}}{V} = 0 \qquad (Boyle) \tag{1}$$

P is the pressure change of volume V as a result of an external pressure change P_e. F_e represents the volume flux leaving the inlet. The acoustic resistance of the inlet is R. See figure AI 1.

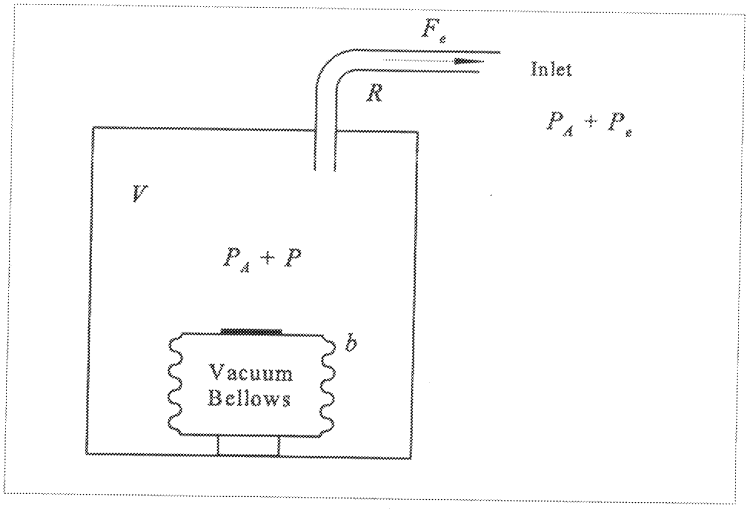

Figure AI 1.
Schematic diagram of an absolute microbarograph. The volume is V, P_A is the ambient pressure, P_e is external pressure, P is the internal pressure change, F_e is the volume flux, R is the resistance of the inlet port and b is the volume change per unit of pressure change of the bellows.

The formulation above corresponds to isothermal processes. Strictly speaking, this is only valid for processes with an efficient heat exchange with the surroundings, such as low frequency processes in narrow volumes. In other cases, however, it is more appropriate to use the equations for adiabatic processes instead of Boyle's Law:

$$P_A V^{\gamma} = constant \quad ; \quad \frac{\dot{P}}{P_A} + \gamma \frac{\dot{V}}{V} = 0 \quad ; \quad \gamma = C_p / C_v \qquad (Adiabatic) \tag{1a}$$

Using equation (1a) it then follows that:

$$\frac{\dot{P}}{P_A} + \gamma\frac{b\dot{P}}{V} + \gamma\frac{P-P_e}{RV} = 0 \quad with \quad \dot{V} = \frac{P-P_e}{R} \quad ; \quad dV = b\,dP \tag{2}$$

The volume of the microbarograph can be seen as being in communication with the pressure outside through an air piston. When the inside pressure P increases the volume also increases. This explains the sign of the second equation in (2).The constant b is defined as the volume increase dV of the bellows when the pressure increases with one unit of pressure dP. The response and the input resistance of the system are given by:

$$D = \frac{P}{P_e} \quad , \quad \Omega = \frac{P_e}{F_e} \tag{3}$$

For the time dependence a harmonic signal can be used: $d/dt = i\omega$.

$$\frac{i\omega P}{P_A} + \gamma\frac{b\,i\omega P}{V} + \gamma\frac{P}{RV} - \gamma\frac{P_e}{RV} = 0 \tag{4}$$

The response is finally given by:

$$D = \frac{1}{i\omega R(V/\gamma)\,\alpha + 1} \qquad where \qquad \alpha = \frac{1}{P_A} + \frac{b}{V} \tag{5}$$

To calculate the input impedance it follows from (2) that:

$$\frac{\dot{P}}{P_A} + \gamma\frac{b\dot{P}}{V} + \gamma\frac{F_e}{V} = 0 \qquad where \;\; P = RF_e + P_e \tag{6}$$

Eliminating the pressure P:

$$\frac{R\dot{F}_e}{P_A} + \frac{\dot{P}_e}{P_A} + \gamma\frac{bR\dot{F}_e}{V} + \gamma\frac{b\dot{P}_e}{V} + \gamma\frac{F_e}{V} = 0 \qquad where \;\; \dot{P} = R\dot{F}_e + \dot{P}_e \tag{7}$$

After division by F_e and $d/dt = i\omega$ and using (3), the input impedance is given by:

$$\Omega = \frac{-1}{i\omega(V/\gamma)\,\alpha} - R \tag{8}$$

The negative sign of the impedance Ω is due to the choise of the sign of F_e. It is clear that the impedance is the sum of a resistance R and a complex volume term. If b is set to zero, it follows that the volume term is given by:

$$\Omega_V = \frac{1}{i\omega(V/\gamma)(1/P_A)} \tag{9}$$

This term is identical to the more usual formulation:

$$\Omega_V = \frac{1}{i\omega C} = \frac{1}{i\omega(V/\rho c^2)} = \frac{1}{i\omega(V/\gamma P_A)} \qquad where \quad c^2 = \gamma\frac{P_A}{\rho} \tag{10}$$

To determine the frequency band to which the adiabatic or isothermal theory applies, experiments can be performed like those of the classic Clement and Desormes experiment for the measurement of $\gamma = C_p/C_v$ in physical chemistry. See appendix VII.

Appendix II *Determination of the acoustic resistances*

The acoustic resistance is defined just like Ohm's Law $R = V / I$:

$$R_a = \frac{P}{dv/dt} \tag{1}$$

R_a is the acoustic resistance, P is the pressure difference across the resistance and dv/dt is the volume velocity. The measurement of R_a involves determination of P and dv/dt.

The measurement of acoustic resistances follows the same procedure as the classical experiment in physical chemistry for the determination of gas viscosity. Figure AII 1 shows the instrumental set-up after Grover (1971). In the experiment water from a reservoir is fed with a slow but constant flow into the expansion volume through the inlet valve to generate a constant pressure by which air escapes through the "device under test". This can be a porous hose or a capillary inlet port. The water reservoir is set a few meters higher than the water level in the expansion volume to generate a constant water pressure at the inlet valve. By lowering the water reservoir below the water level in the expansion volume, the experiment can be performed with underpressure instead of overpressure. The set-up with water from a reservoir is to ensure a constant temperature in the experiment since the water is allowed to settle at room temperature.

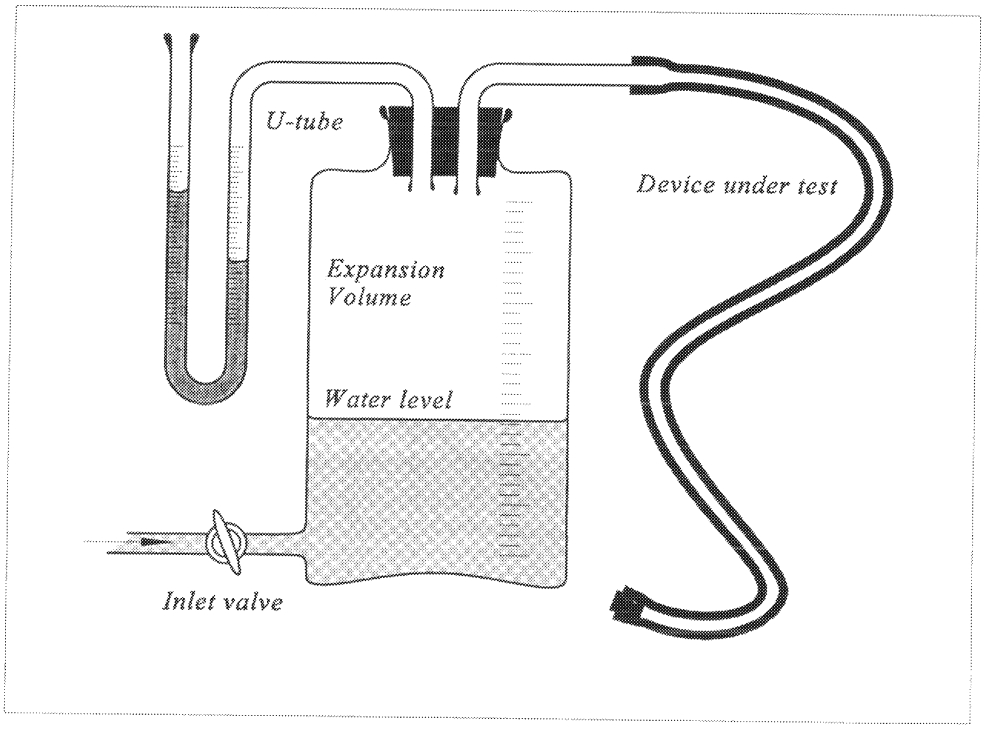

Figure AII 1.
Instumental set-up for the determination of acoustic resistance.

The equipment can measure the volume velocity by timing the volume change with the aid of the graduation on the expansion volume. The pressure is measured with the U-tube manometer.

From the theory (Moore, 1972) it is well known that for gases capillary flow in a tube is described by Poiseuille's Law, which is given by:

$$\frac{dv}{dt} = \frac{\pi (P_1^2 - P_2^2)\, a^4}{16 l \eta P_0} \tag{2}$$

dv/dt is the volume velocity measured at pressure P_0, P_1 and P_2 are fore and back pressures respectively, η is the viscosity of air (182.7 micropoises at 18 ^{0}C), a is the radius of the capillary with length l. In this experiment P_0 is equal to P_1. With $P = P_1 - P_2$ and $P_1 = P_0$ equation (2) becomes:

$$\frac{dv}{dt} = \frac{\pi P a^4}{8 l \eta} - \frac{\pi P^2 a^4}{16 l \eta P_0} = \frac{\pi P a^4}{8 l \eta}\left(1 - \frac{P}{2P_0}\right) \tag{3}$$

The second term is small for acoustic pressures. Within the limits of small pressure differences P the equation reduces to the familiar Poiseuille value for incompressible fluids:

$$R_a = \frac{P}{dv/dt} = \frac{8 l \eta}{\pi a^4} \tag{4}$$

In figure AII 2 the experimental results are plotted for a porous hose (Soaker Hose made by Hoze Lock or Gardena) of 1 meter length and an inside diameter of 12 millimeters. The results for a 5/8 inch hose (by Moisture Master) indicate a lower resistance.

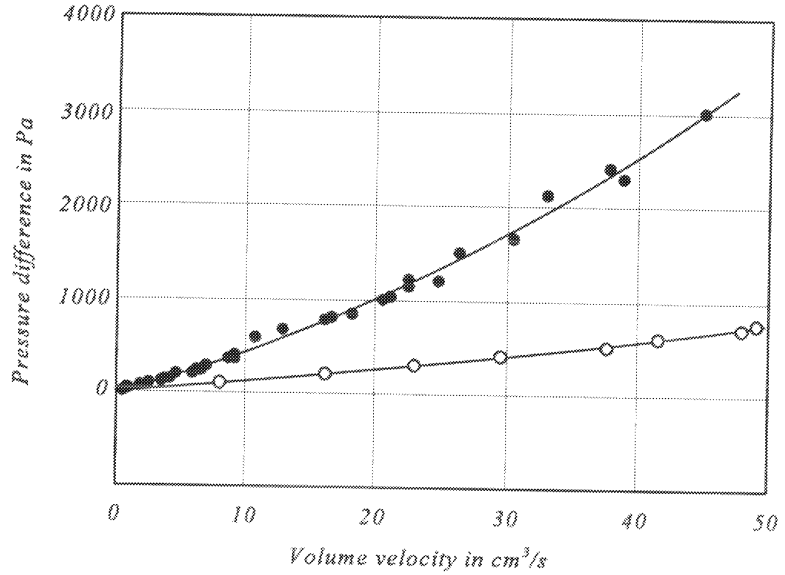

Figure AII 2.
Pressure difference versus volume velocity to determine the acoustic resistance of a porous hose with a length of 1.0 m and an inside diameter of 12 mm (closed circles), and 16 mm (5/8 in) (open circles).

Figure AII 2 clearly shows a quadratic dependence instead of the expected linear dependence. Note, however, that a porous hose has a distribution of complicated capillaries that constitute the acoustic resistance and has not single straight capillaries. So a purely parabolic velocity profile across the diameter of the capillaries, as simple theory proposes, might be disturbed. Furthermore, there is a pressure drop as a result of fluid velocity given by Bernoulli's Law:

$$\Delta P = \frac{\rho}{\pi^2 a^4} (dv/dt)^2 \qquad (5)$$

This quantity is known as the kinetic energy correction (Schoemaker et al., 1967). In practice, ΔP is subtracted from the overall pressure difference P. This is the main contribution to the quadratic dependence between the pressure difference and the volume velocity.

Finally the above theory assumes laminar flow. It has established empirically that for a long round straight tube laminar flow is observed when the Reynolds number does not exceed the value of 2300. In this case the Reynolds number *Rey* is defined as:

$$Rey = \frac{d v_{av}}{\nu} = \frac{d v_{av} \rho}{\eta} = \frac{4 f_v}{\pi d} \frac{\rho}{\eta} \qquad (6)$$

In which d is the tube diameter, v_{av} the average air velocity, ρ the density, η the dynamic viscosity, ν the kinematic viscosity and f_v the volume velocity. For small d or for high volume velocities the flow can easily be turbulent instead of laminar.

From figure AII 2 for the 1 meter porous hose (12 mm) the acoustic resistance R_a at low pressure was measured as 3.8 10^7 kg/ m^{4}s, in cgs-units: 380 acoustic ohms. At 1000 Pa pressure difference the resistance is of the order of 500 acoustic ohm meters. Measurements were also performed on wet and moist porous hose in order to estimate the decrease in porosity due to the water content. The resistance increased from 380 to 620 acoustic ohm meters in a moderately wet situation. For the 5/8 inch hose the resistance was measured as 100 acoustic ohm meters.

Higher overpressure results in larger resistance, so non-linear effects will be important. As explained above this effect is caused by the air velocity through the capillaries. When a certain resistance value can be obtained in different ways, the non-linear effects can be diminished by using capillaries that are as wide and long as possible to lower the average air velocity. Note that in the differential pressure barograph the leak resistor between the two volumes in this instrument can be a source of non-linearity.

Other methods of measuring porosity are described in Zwikker et al. (1949), including a method with 2% accuracy based on an analytical balance (Leonard, 1946).

Finally, special attention is given to gas viscosity. Air has the property of being compressible. Therefore the equations that deal with gas viscosity are slightly different from that of incompressible fluids. Derivation of the equation for gas viscosity in a narrow tube starts from Poiseuille's Law for an incompressible fluid:

$$\frac{dv}{dt} = \frac{\pi a^4}{8\eta}\frac{(P_1 - P_2)}{l} \tag{7}$$

The molar rate flow (moles per unit of time) is given by:

$$\frac{dn}{dt} = \frac{P}{RT}\frac{dv}{dt} = \frac{P}{RT}\frac{\pi a^4}{8\eta}\left(-\frac{dP}{dz}\right) = \frac{\pi a^4}{16\eta RT}\left(-\frac{d(P^2)}{dz}\right) \tag{8}$$

with $PV = nRT$. The distance along the tube with length l is denoted as z. In (8) the third term with dP/dz is the differential pressure drop along z and is derived from $(P_1-P_2)/l$ in (7).

Since conservation of matter requires that the mole rate of flow be constant along the tube, $d(P^2)/dz$ must be constant in the last section of (8). Accordingly we can write:

$$\frac{d(P^2)}{dz} = \frac{(P_1^2 - P_2^2)}{l} \tag{9}$$

With this we obtain:

$$\frac{dn}{dt} = \frac{\pi (P_1^2 - P_2^2)\, a^4}{16 l \eta RT} \tag{10}$$

When the volume velocity is measured at pressure P_0, the reverse operation as in (8) is followed. Then going back volume velocities:

$$\frac{dv}{dt} = \frac{\pi (P_1^2 - P_2^2)\, a^4}{16 l \eta P_0} \tag{11}$$

Using this, the equation for gas viscosity is derived. In practice the quadratic term is small compared to the effects of flow velocity as described with Bernoulli's Law.

Leonard, R. W., Simplified Flow Resistance Measurement,
J. acoust. Soc. Am., **17**, 240-241, 1946.

Moore, W. J., Physical Chemistry, 5ed., p 152-154, Longman, 1972.

Shoemaker, D. P., and C. W. Garland, Experiments in Physical Chemistry, 2ed., p 77-86, McGraw-Hill Kogakusha, ltd., 1967.

Zwikker, C., and C. W. Kosten, Sound Absorbing Materials, Elsevier, 1949.

Appendix III *Array responses of triangular and square arrays leaving out one element*

The following illustrations show array responses of triangular and square arrays leaving out one element. The objective is to show the better performance of square arrays in this respect.

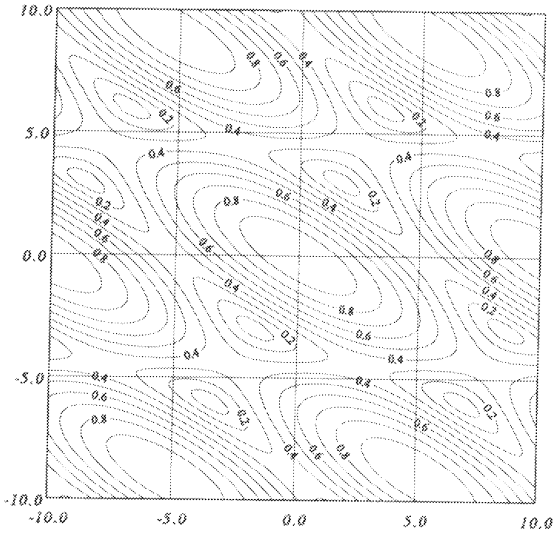

Figure AIII 1.
Response of triangular array minus the corner element.

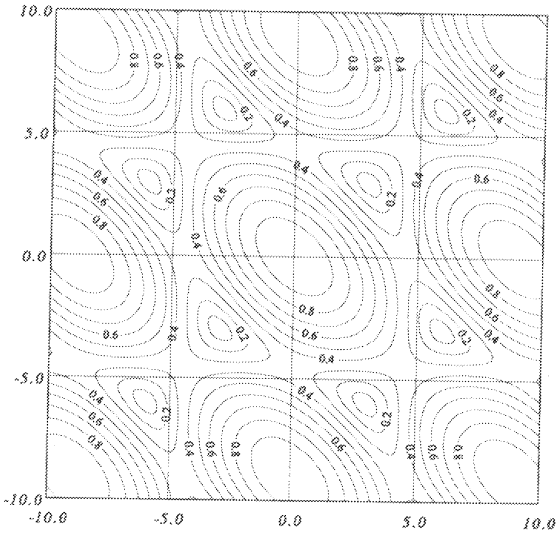

Figure AIII 2.
Response of square array minus the corner element.

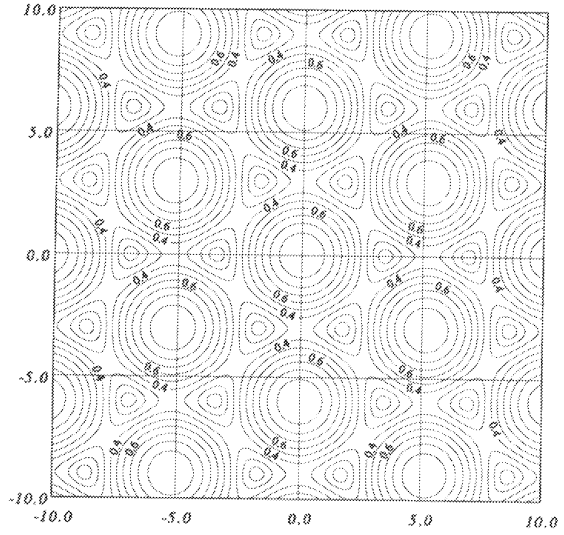

Figure AIII 3.
Response of triangular array minus the centre element.

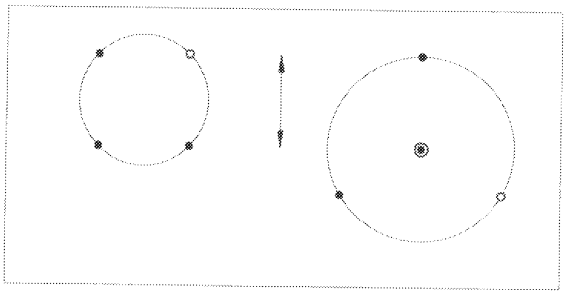

Figure AIII 6.
Array layouts for a square (left) and a triangular array (right). The smallest distance between the array elements is the same for the two configurations. The open circles represent missing elements. The arrow indicates the smallest distance between array elements. In this example the smallest distance is 1000 m.

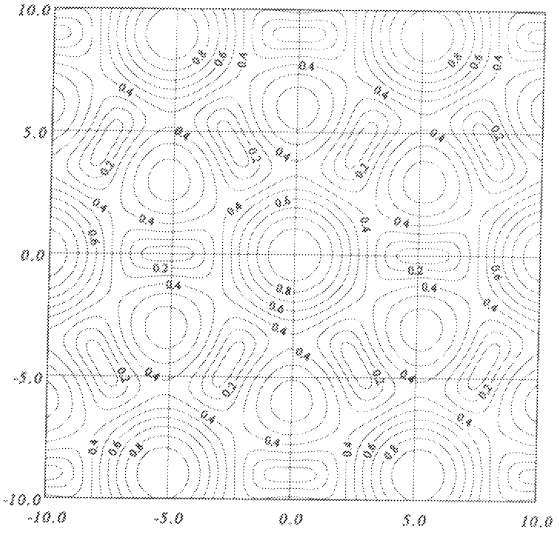

Figure AIII 4.
Response of a complete triangular array.

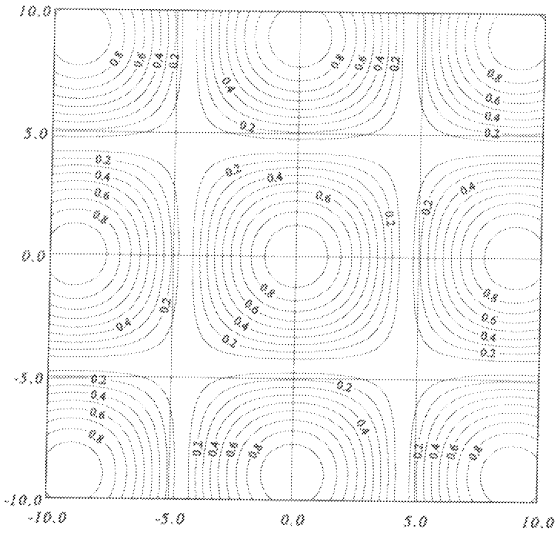

Figure AIII 5.
Response of a complete square array.

The above figures show various responses of arrays that can be used in an infrasound detection system. Figures AIII 4 and AIII 5 show the responses of the complete triangular and square arrays respectively. Figures AIII 1, AIII 2 and AIII 3 give the responses of triangular and square arrays with one element missing. The figures AIII 1 through AIII 5 all plot the power of the response versus horizontal slowness in s/km along the axes. All responses are calculated for a wavelength of 3 km or a frequency of 0.11 Hz. Figure AIII 6 gives an overview of the array configurations. The smallest distance is 1000 m.

There is a trade off between the slightly better resolution of the triangular array and the lower performance when one element is missing. In all cases the proposed arrays have rather poor responses due to the very limited number of elements.

In an array two distances are important. The smallest distance between the array elements determines the distance between the main lobe and the side lobes. The largest distance in the array determines the resolution of the main lobe. In any comparison between arrays there is a choice leaving one of the two distances the same. This argument also colors the discussion on how large an infrasonic arrays must actually be. When the number of elements is fixed to four, a larger array will enhance the resolution while at the same time the side lobes are found at lower values of slowness. The whole pattern of the array response is reduced. The pattern is shaped by the product of ωpr.

For example, in figure AIII 7 the response of a six-element array is depicted. A full discussion of these types of arrays is given by Haak (1996). It is clear that a six-element array has a better separation between side lobes and the main lobe irrespective of the overall dimension of the array. Figure AIII 8 illustrates the array configuration.

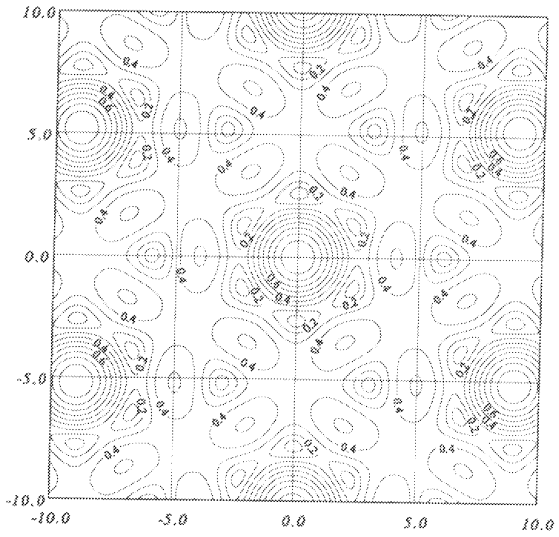

Figure AIII 7.
Response of a six-element array.
Note that a six-element array is larger than the two four-element arrays when the resolution is fixed.
The resolution depends on the total array dimension. The distance of the main lobe to the nearest side lobes depends on the smallest array element distance.

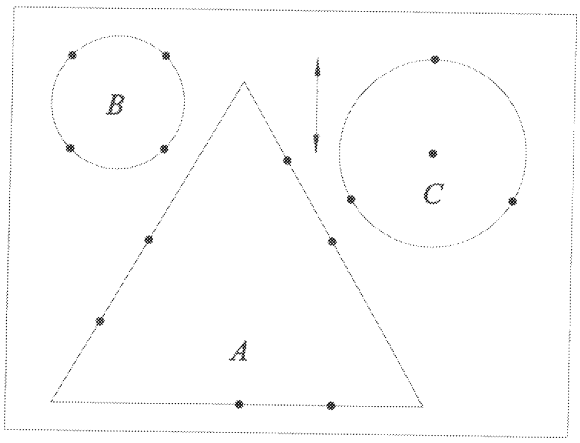

Figure AIII 8.
Array layout of a six-element array (A). For comparison also the other arrays are drawn. The arrow represents the smallest distance of 1000 m between the array elements.

Appendix IV *Short theory of sound propagation in tubes*

In this appendix the simplified theory of sound propagation in tubes with rigid and non-heat conducting walls is given. It is assumed that the particle velocity is the same over the entire cross-section of the tube, i.e. plane waves, that the friction is proportional to the particle velocity and
that the diameter of the tube is considerably less than the wavelength. This derivation follows Rschevkin (1963).

Consider a small volume element $\Delta v = S\Delta x$ bounded by two planes x_1 and $x_2 = x_1 + \Delta x$. Traversed by a longitudinal sound wave the layer of particles with coordinate x_1 is shifted by a quantity ξ. See figure AIV 1 for details.

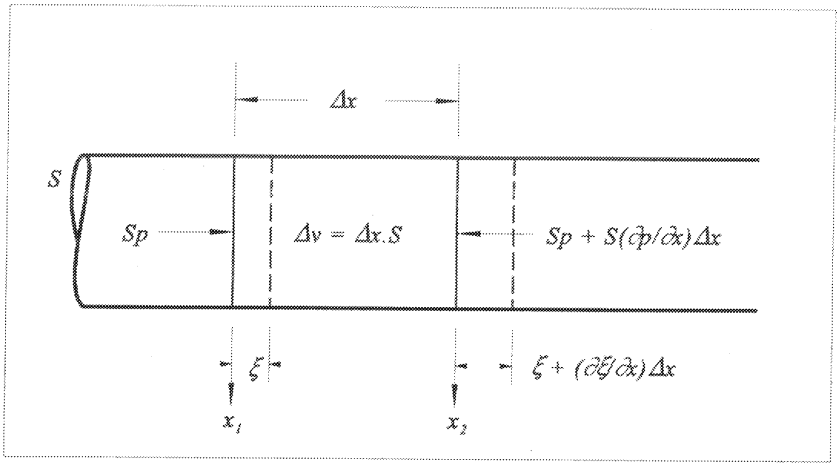

Figure AIV 1.
Longitudinal particle displacement inside a tube.

The wave equation of sound propagation can be derived from the forces that are present in the process. The inertial forces are given by the mass and the acceleration of the volume element:

$$F_i = \rho \Delta x S \frac{\partial^2 \xi}{\partial t^2} \qquad (1)$$

The frictional forces are assumed to be proportional to the particle velocity:

$$F_f = r \Delta x S \frac{\partial \xi}{\partial t} \qquad r = \frac{8\mu}{a^2} : \ Poiseuille \ ; \quad r = \frac{1}{a}\sqrt{2\rho\mu\omega} : \ Stokes-Helmholtz \qquad (2)$$

The parameter r is the friction coefficient. The Poiseuille dependence of r is applicable to small diameters or low frequencies. The Stokes - Helmholtz dependence of r is applicable to large diameters or high frequencies. The tube radius is a.

The force due to the difference of pressures on both sides of the volume element amounts to:

$$F_x = -S\frac{\partial p}{\partial x}\Delta x \tag{3}$$

The pressure can be rewritten in the assumed adiabatic process with the following relations:

$$p = -\kappa\frac{\delta v}{\Delta v} = -\kappa\frac{\partial \xi}{\partial x} \quad ; \quad \kappa = \gamma P_0 = \rho c^2 \quad ; \quad Y = \frac{1}{\kappa} = -\frac{1}{V}\frac{\partial v}{\partial p} \tag{4}$$

For a gas the bulk modulus is indicated by κ, P_0 is the static pressure and Y is the compressibility. The total force on the volume element can also be written as:

$$F_x = S\kappa\frac{\partial^2 \xi}{\partial^2 x}\Delta x \tag{5}$$

Now the equation of motion can be derived taking into account both pressure and frictional forces. For the moment thermal effects are neglected. The equation of motion is given by:

$$\rho S\Delta x\frac{\partial^2 \xi}{\partial t^2} + rS\Delta x\frac{\partial \xi}{\partial t} - \kappa S\Delta x\frac{\partial^2 \xi}{\partial x^2} = 0 \tag{6}$$

In order to get an equation per unit of length (6) is divided by Δx; to get an equation in terms of pressures instead of forces (6) is divided by S:

$$\rho\frac{\partial^2 \xi}{\partial t^2} + r\frac{\partial \xi}{\partial t} - \kappa\frac{\partial^2 \xi}{\partial x^2} = 0 \tag{7}$$

In order to get an equation in terms of volume fluxes f, (7) is differentiated with respect to time and the equation is again divided by S:

$$\frac{\rho}{S}\frac{\partial^2 f}{\partial t^2} + \frac{r}{S}\frac{\partial f}{\partial t} - \frac{\kappa}{S}\frac{\partial^2 f}{\partial x^2} = 0 \tag{8}$$

This equation can now directly be compared to the Telegraphist's Equation, see also appendix V, given the expressions for r and κ:

$$\frac{\rho}{S}\frac{\partial^2 f}{\partial t^2} + \frac{8\mu}{\pi a^4}\frac{\partial f}{\partial t} - \frac{\rho c^2}{S}\frac{\partial^2 f}{\partial x^2} = 0 \tag{9}$$

The analogue expression for an electronic circuit reads:

$$M\frac{\partial^2 f}{\partial t^2} + R\frac{\partial f}{\partial t} - \frac{1}{C}\frac{\partial^2 f}{\partial x^2} = 0 \tag{10}$$

The volume flux f can be associated with an electric current i. The parameter M is the inductance per unit length, the coil in the circuit or the inertance per unit length in the mechanical representation. R is the resistance per unit length. C represents the compliance per unit length, the condensator in the circuit.

The same type of equation applies to the pressure of the system. Starting from particle displacement we can go to volume flux with:

$$f = S\frac{\partial \xi}{\partial t} \tag{11}$$

or to pressure with:

$$p = -\kappa\frac{\partial \xi}{\partial x} \tag{12}$$

So the equation of motion in terms of pressure reads:

$$M\frac{\partial^2 p}{\partial t^2} + R\frac{\partial p}{\partial t} - \frac{1}{C}\frac{\partial^2 p}{\partial x^2} = 0 \tag{13}$$

The following relations are derived by comparing equations (9) and (10):

$$M = \frac{\rho}{S} \quad ; \quad R = \frac{8\mu}{\pi a^4} \quad ; \quad \frac{1}{C} = \frac{\rho c^2}{S} \tag{14}$$

The solution of the equation of motion is a wave:

$$\xi_t = \xi_{ot} e^{i\omega t} e^{\pm \Gamma x} \tag{15}$$

where ξ_t is the particle velocity, Γ is the propagation constant and ω is the frequency. Γ can be written as $\alpha + i\beta$. The real part characterizes the attenuation of the wave amplitude per unit path length and is known as the damping factor. The imaginary part is the wave number, which determines the phase speed, hence in tubes dispersion occurs. Γ can be found with equations (15) and (12):

$$\Gamma = \sqrt{(r + i\omega\rho)(i\omega/\kappa)} \tag{16}$$

For the pressure wave in the tube moving to the right we find using equations (7) and (12):

$$p(x,t) = \xi_{ot}\frac{e^{-\Gamma x} e^{i\omega t}}{\Gamma}(r + i\omega\rho) \quad ; \quad p(x,t) = \xi_t z \quad ; \quad z = \frac{(r + i\omega\rho)}{\Gamma} \tag{17}$$

Since this equation contains the pressure and the particle velocity, (17) also defines the specific acoustic impedance (pressure/particle speed).

In part reproduced from: Rschevkin, S. N., The theory of sound, Pergamon Press, 1963.

Appendix V *Theory of electric transmission lines*

Consider an electric transmission line with distributed inductance L, capacitance C, resistance R and conductance G, as given in figure AV 1. The voltage and current changes across the line element length δx are: (Telegraphist's Equations)

$$\frac{\partial V}{\partial x} = -L\frac{\partial I}{\partial t} - RI = -(R + i\omega L)I \qquad \frac{\partial I}{\partial x} = -C\frac{\partial V}{\partial t} - GV = -(G + i\omega C)V \tag{1}$$

When harmonic dependence of time is assumed V and I are given by:

$$V = V_0 e^{i\omega t} \qquad I = I_0 e^{i\omega t} \tag{2}$$

Eliminating V (or I) in equations (1), the second order differential equations are obtained:

$$\frac{\partial^2 V}{\partial x^2} = \Gamma^2 V \qquad \frac{\partial^2 I}{\partial x^2} = \Gamma^2 I \quad with \quad \Gamma = \sqrt{(R+i\omega L)(G+i\omega C)} \tag{3}$$

Γ is the propagation constant. The solution of (3) is given by:

$$V = (Ae^{-\Gamma x} + Be^{\Gamma x})e^{i\omega t} \qquad I = \frac{(Ae^{-\Gamma x} - Be^{\Gamma x})}{Z}e^{i\omega t} \tag{4}$$

The solution for the current I is found by using the solution for V and equation (1). Z is the characteristic impedance of the transmission line, defined as the ratio of voltage and current:

$$Z = \sqrt{\frac{R + i\omega L}{G + i\omega C}} \tag{5}$$

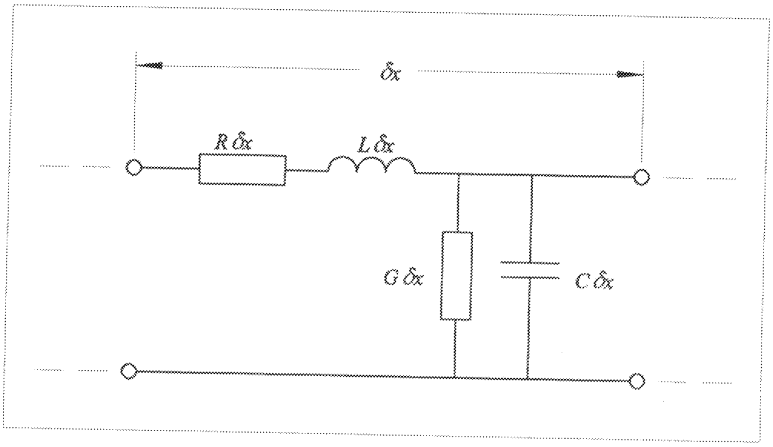

Figure AV 1.
Transmission line element.

See also: Carter, G. W., and A. Richardson, Techniques of circuit analysis, Cambridge, 1972, and Owen, G. W., and P. W. Keaton, Fundamentals of Electronics, Vol. I, p 254, Harper International Ed., 1966.

Appendix VI *Noise reducer response*

In this appendix an alternative to the theory as put forward by Burridge (1971) is presented. The theory describes a complete microbarograph system. The two alternatives differ in approach. Here a theory is given that treats specifically one arm of the noise reducer, together with the other side branches and the microbarograph. The calculations are somewhat more consistent with standard theory and calculations of porous hose with a continuous inlet are made easier. In figure AVI 1 an overview is given.

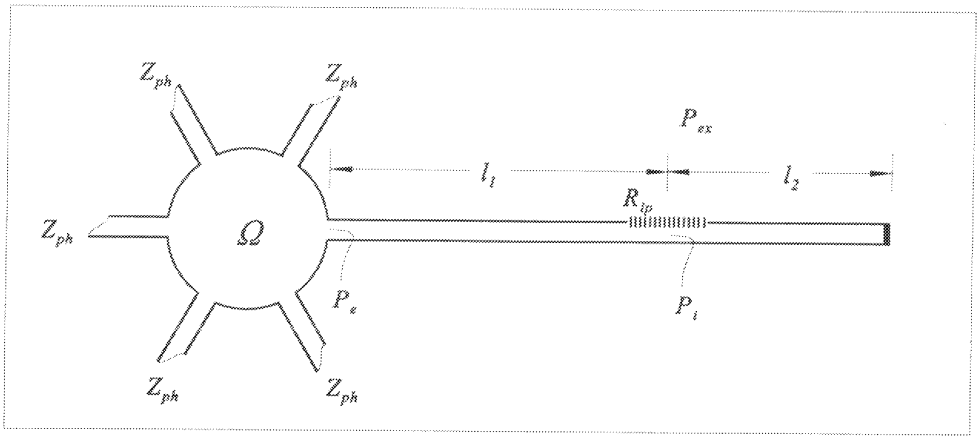

Figure AVI 1.
Acoustic scheme of the microbarograph and noise reducer.

The first step is to calculate the pressure inside the tube as a result of one unit harmonic pressure outside. This outside pressure is applied at a distance l_1 from the microbarograph inlet and it is assumed to be limited to one meter in length. In a continuous system no discrete inlet ports exist as is the case in the Burridge article:

$$P_i = P_{ex} \frac{Z_t}{R_{ip} + Z_t} \qquad (1)$$

In this equation P_i is the pressure just inside the tube, P_{ex} is the external pressure, Z_t is the total impedance at this point just across the point of entry defined by l_1 and l_2 which add up to l_t. The impedance R_{ip} is given by the porosity of the tube. In this study it is determined as 380 cgs acoustic units for one meter (see appendix II). The total impedance Z_t is given by the impedances of the two branches of the line to the left and to the right from R_{ip}, both terminated with their own terminating impedances:

$$Z_t = \frac{Z_1 Z_2}{Z_1 + Z_2} \qquad (2)$$

Z_1 and Z_2 are the two impedances of the two branches of the noise reducing structure as seen from the point of pressure input. Both impedances are terminated with characteristic loading impedances. Z_2 depends on the impedance Z_0 of the tube itself, the propagation constant Γ and a infinite impedance terminator when a stopper at the end is applied:

$$Z_2 = Z_0 \frac{\cosh(\Gamma l_2)}{\sinh(\Gamma l_2)} \tag{3}$$

For the other branch of the noise reducer arm the calculation is more complicated, it involves not only the input impedance of the barograph Ω, but also the loading impedances Z_{ph} of the five other branches of the noise reducing structure:

$$Z_1 = Z_0 \left[\frac{Z_0 \sinh(\Gamma l_1) + Z_L \cosh(\Gamma l_1)}{Z_0 \cosh(\Gamma l_1) + Z_L \sinh(\Gamma l_1)}\right] \tag{4}$$

Z_L is given by:

$$Z_L = \frac{\Omega Z_{ph}/5}{\Omega + Z_{ph}/5} \quad ; \quad Z_{ph} = Z_0 \frac{\cosh(\Gamma l_1)}{\sinh(\Gamma l_1)} \tag{5}$$

Now P_{ex} is set to be 1.0 Pa. Then via (1) P_1 is given. After that P_e can be calculated via:

$$P_e = P_1 \left[\cosh(\Gamma l_1) + \frac{Z_0}{Z_L} \sinh(\Gamma l_1)\right]^{-1} \tag{6}$$

Finally :

$$\Delta = D P_e \quad ; \quad Resp = \frac{\Delta}{1.0\ Pa} \tag{7}$$

D is the response of the microbarograph itself as given in appendix I and Δ is the response of the complete microbarograph system to a unit pressure pulse at the input of the system. In this formulation it is dependent on the distance l_1 from the microbarograph. It is also a function of frequency.

With the reciprocity principle the response of the system can be calculated to plane waves as a function of slowness and azimuth. The response function A of the microbarograph and noise reducer is given by:

$$A(\omega, \vec{p}) = \int_{nr} \Delta(\omega, \vec{r})\, e^{i\omega \vec{p} \cdot \vec{r}} d\vec{r} \qquad with \qquad \vec{p} = \frac{\hat{l}}{c} \tag{5}$$

The integral is taken over the porous hose section of the noise reducer (nr), c is the speed of sound in air, p is the slowness vector.

Appendix VII *Experiment of Clement and Desormes*

This classical experiment in physical chemistry can help to determine at what frequency the adiabatic regime changes over to the isothermal regime. In short this experiment measures the C_p/C_v ratio by a three step process. First a volume of gas is given an overpressure. The second step is a fast expansion during which the temperature changes. The third step is a slower equalisation of temperature. In this step the temperature is monitored by the pressure of the gas.

For a reversible process under adiabatic conditions, the energy change of a gas is given by:

$$dE = -p\,dV \tag{1}$$

For a perfect gas the equation of state for pressure p and volume V is:

$$p\,V = n\,R\,T \tag{2}$$

The constant R is the universal gas constant, n is the number of moles and T the temperature.

While E for a perfect gas is a function of temperature alone, the energy change is given by:

$$dE = C_v\,dT \tag{3}$$

In which C_v is the heat capacity at constant volume. Substitution of equations (2) and (3) in (1) will result in :

$$C_v \frac{dT}{T} = -n\,R \frac{dV}{V} \tag{4}$$

After integration and changing the extensive parameters to: $c_v = C_v / n$ and $v = V / n$. The following relation is obtained:

$$c_v\,ln\frac{T_2}{T_1} = -R\,ln\frac{v_2}{v_1} \tag{5}$$

This equation is fundamental to the experiment.

Now the experiment can be carried out. First the volume v_1 is given a pressure of P_1 and is allowed time to stabilise to temperature T_1. In the second step the gas is expanded adiabatically and reversible to a pressure P_2. The state of the gas A will then change :

$$A\,(P_1,v_1,T_1) \rightarrow A\,(P_2,v_2,T_2) \tag{6}$$

Now:

$$\frac{T_2}{T_1} = \frac{P_2}{P_1}\,\frac{v_2}{v_1} \tag{7}$$

Substitution of (7) into (5) gives:

$$\ln\frac{P_2}{P_1} = -\frac{c_v+R}{c_v} ln\frac{v_2}{v_1} = -\frac{c_p}{c_v} ln\frac{v_2}{v_1} \tag{8}$$

with for a perfect gas:

$$c_p = c_v + R \tag{9}$$

In the third step the system is given time to adjust to the ambient temperature T_1 and the temperature is measured by monitoring the pressure at constant volume:

$$A(P_2,v_2,T_2) \rightarrow A(P_3,v_2,T_1) \tag{10}$$

Now applying Boyle's Law to the first and the third step both at temperature T_1:

$$\frac{v_2}{v_1} = \frac{P_1}{P_3} \tag{11}$$

Insertion of (11) in (8) gives:

$$\gamma \ln\frac{P_1}{P_3} = -ln\frac{P_2}{P_1} \quad ; \quad \gamma = \frac{ln\,P_1 - ln\,P_2}{ln\,P_1 - ln\,P_3} \tag{12}$$

In practice the experiment is simple when the absolute pressure microbarograph is used. The noise reducer tubes inlets of the barograph are closed except one. A piston is attached to the inlet such as a syringe. With this the pressure step can be generated. When the pressure is changing from P_2 to P_3 the time response can be measured and can be fitted to the function $e^{-\alpha}$ (see figure AVII 1). The time constant is $1/\alpha$. It is essential that the microbarograph is free of any leaks.

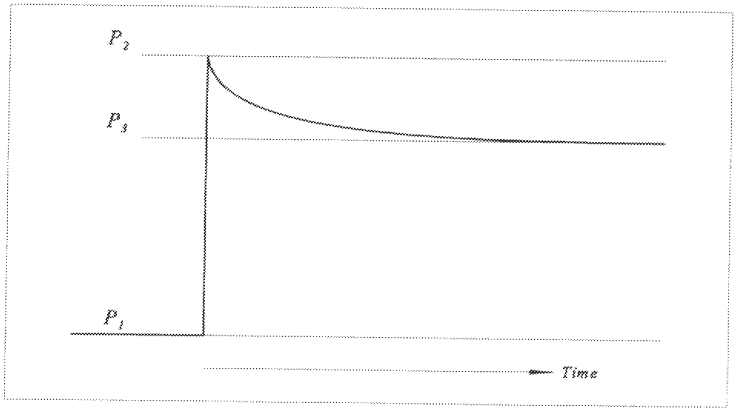

Figure AVII 1.
Pressure vs time in the Clement and Desorme experiment.

In part reproduced from: Shoemaker, D. P., and C. W. Garland,
Experiments in Physical Chemistry, p 61- 67, 2ed., McGraw-Hill Kogakusha, ltd., 1967.

Appendix VIII *Wave propagation in a closed flexible tube*

When a pressure wave is travelling through a flexible tube, the walls are responding to the pressure with a change of the radius. Derivation of the equations for wave propagation in a flexible tube starts with the electric analogue of an acoustic transmission line with the differential equations for pressure and volume flux:

$$\frac{\partial p}{\partial x} = -L\frac{\partial f}{\partial t} - Rf = -(R + i\omega L)f \qquad \frac{\partial f}{\partial x} = -C\frac{\partial p}{\partial t} - Gp = -(G + i\omega C)p \tag{1}$$

For simplicity assume $Gp = 0$ for a closed tube neglecting thermal effects. In the case of an elastic tube there are two contributions to the transverse flux f: an elastic contribution of the tube wall and an inertial contribution of the moving mass of the wall.

Focussing on the second part of (1), describing the fluxes f per unit length, an expression can be found for the yielding of the tube by the inside pressure p. If the stiffness of the tube wall K_w is defined as:

$$K_w = \frac{S}{dS}p \tag{2}$$

The cross-section of the tube is S, so K_w is the ratio of the pressure change and the fractional change in cross-section. The volume change over a short length of tube dx is:

$$dV = dx\,dS = \frac{dx\,S\,p}{K_w} \tag{3}$$

Differentiation with respect to time and notation per unit length result in an elastic flux:

$$\frac{\partial f_e}{\partial x} = \frac{S}{K_w}\frac{\partial p}{\partial t} = \frac{S}{K_w}i\omega p \tag{4}$$

The complex elastic admittance per unit length Y_e is therefore given by:

$$Y_e = \frac{\partial f_e/\partial x}{p} = \frac{S}{K_w}i\omega \tag{5}$$

So equation (1) can read with $Gp = 0$ and including the compressibility of air:

$$\frac{\partial f}{\partial x} = -S\left(\frac{1}{\rho c^2} + \frac{1}{K_w}\right)\frac{\partial p}{\partial t} \tag{6}$$

The inertial contribution due to the moving mass of the tube wall can also be calculated. In this example a constant wall thickness d_w of the tube is assumed. The complex inertial admittance per unit length Y_i is given by:

$$Y_i = \frac{\partial f_i/\partial x}{p} = \frac{2\pi a\,\frac{\partial a}{\partial t}}{d_w\rho\,\frac{\partial^2 a}{\partial t^2}} = \frac{2\pi a}{d_w\rho}\frac{1}{i\omega} = \frac{(2\pi a)^2}{m\,i\omega} = \frac{4\pi S}{m\,i\omega} \tag{7}$$

The density of the tube wall material is ρ, a is the radius and m is the mass per unit length. The numerator of (7) is the volume change with time per unit length. The denominator is the inertial force per area; the inertial pressure.

Going back to (1) $Gp = 0$ can be replaced by the reciprocal sum of the two contributions:

$$\frac{Y_e Y_i}{Y_e + Y_i} p = i\omega S (K_w - m\omega^2/4\pi)^{-1} p \tag{8}$$

In this approach the damping of the second order system is neglected. It can be reinstalled by introducing a term proportional to p, since damping involves a force proportional to volume flux f. Equation (8) introduces a resonance frequency with the value:

$$\omega_0^2 = \frac{K_w 4\pi}{m} \tag{9}$$

The resonance frequency should be higher than the frequency range of interest, otherwise the response of the closed tube will be far from flat. In any case the elastic yielding of the wall will result in a slight dispersion of the transmitted wave.

Since there are now two stiffnesses involved they can be described together, so C in equation (1) as defined in equation (6) can now also be written as:

$$C_e = \frac{S}{\rho c^2} \frac{\omega_1^2 - \omega^2}{\omega_0^2 - \omega^2} \qquad with \qquad \omega_1^2 = \omega_0^2 + \frac{\rho c^2}{m/4\pi} \tag{10}$$

Where ω_1^2 is the resonant frequency of the wall stiffened by the air inside. For frequencies between ω_1 and ω_0 the propagation of acoustic waves is strongly attenuated.

With soft tube, such as silicon tube, the resonance frequency is usually higher than 50 Hz. In this case no substantial effects of the wave propagation can be seen for frequencies lower than 10 Hz. However, note that, the phase velocity of closed pipes and hoses is lower toward lower frequencies.

The stiffness of the tube wall K_w was measured for a silicon tube of 12 mm inside diameter and a wall thickness of 2 mm. The method used was to fill the tube with water over a length of one meter. The pressure applied to the hose was ± 50 hPa, the fractional change of length of the water column equals the fractional change of the cross-section, since the water volume is constant. The stiffness K_w was measured to be $2.0\ 10^5$ Pa. This is in good agreement with the value of the Young's modulus E for silicones, which is related to K_w by:

$$K_w = \frac{E d_w}{2a} \tag{11}$$

In part reproduced from: Morse, P. M., and K. U. Ingard, Theoretical Acoustics, p 475 and 688, McGraw-Hill (1968).

Appendix IX *Noise reducers with a roof*

Changing from experimental to observatory conditions, stability of operation is needed over extended periods of time. The need for robust solutions to the moist problem increases. With the introduction of porous hose this became even more apparent. In the course of several years we tried different solutions. At least one conclusion was that a lot of testing still has to be done and otherwise that new ideas are often more brilliant than useful. Today we still lack a robust and easy to construct solution to the problem of outside measurement of low level pressures with the aid of noise reducers of considerable length. Reducers that employ capillaries instead of porous materials are not much different in this respect. In several systems we saw a slow change of sensitivity in time. The typical interval between maintenance operations was one year.

For remote parts of the world and in areas of severe climatological conditions, maintenance operations can be a problem. Therefore any robust solution or improvement will be of help to achieve a stable operation over the years. One such solution may be the construction of a small roof over the noise reducer. This solution was first proposed by the infrasound group at LDG. We propose a lower version; figure AIX 1 illustrates this experimental roof.

The roof has several advantages apart from being a shelter to rain, snow, hail and frost. The roof structure lifts the whole noise reducer 10-20 cm from the ground and therefore avoids direct contact with dirt and moist from the soil underneath. When the roof structure is lifted, higher the stronger winds will introduce excess noise. The roof structure is also a protector against small animals such as rodents. Porous hose and flexible closed hose are both vulnerable in this respect.

Apart from the mechanical protection described above the roof is also a good radiation regulator. In sunny weather the roof protects against direct heating by solar radiation and on nights when the sky is clear it prevents excessive cooling by radiation from the noise reducer itself. In this way a milder micro climate is created around the noise reducer.

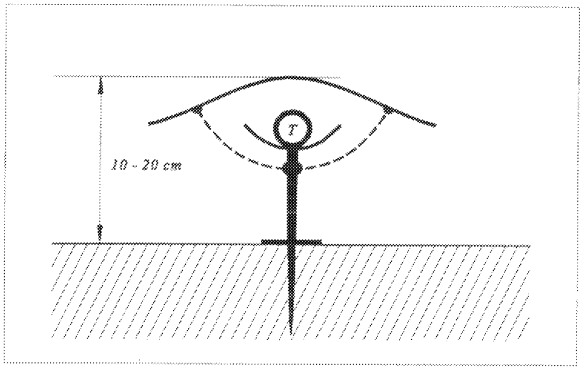

Figure AIX 1.
Impression of a roof over a noise reducing structure. Only the roof and the support of the hose continue all along the porous hose T. Other parts, such as the ground spikes and the roof support wires are present at intervals of one meter.

Appendix X *Circular noise reducers*

Circular noise reducers are described by Grover (1971) and Burridge (1971). Both authors come to the conclusion that circular noise reducers are a good alternative to the more complicated Daniels line microphone. Apparently the easy construction of a circular noise reducer was an important factor. No comparison was made at the time with noise reducers in star formations. The length of tubing is approximately the same for a six-arm star formation and a circular noise reducer of the same radius. In this appendix the results are presented of the full slowness dependence of a circular noise reducer tube after Burridge. Rayleigh (1945) discusses circular tubes with respect to modes, but not for a continuous frequency range.

The structure of the calculations is illustrated in figure AX 1. From the inlet two branches lead to the microbarograph detector, in general of unequal length. The inlet itself is acting as a piston driving the system continuously at a given frequency. The geometry of the system and the propagation constant determine the overall pressure distribution as a result of the pumping action of the piston. The inlets are leaks. The microbarograph is represented as a volume.

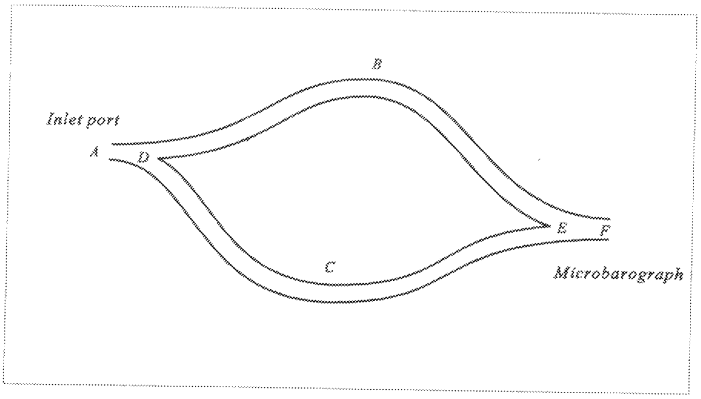

Figure AX 1.
Schematic layout of a circular noise reducer
(after Rayleigh).

In figure AX 1 the situation is depicted in a way that the microbarograph is reached along two paths of different length B and C. The phase difference at E result in a certain amount of interference. The pressure at the microbarograph is sensed through the resistance between E and F. Besides the interference a pressure wave may be reflected back to D through the two braches B and C. Constructive interference can occur when the path length is equal to the wavelength. Destructive interference is noticed with half wavelength differences.

Inlet ports are attenuating the propagating waves inside the tube. Low inlet port resistances will cause strong damping and will result in a rapidly attenuating propagating wave in the tube. In case of low damping a fully developed mode structure is seen at high frequencies. A proper design should avoid ring diameters which are too large in order to have a straightforward response of the noise reducing structure.

The angular dependence of the sensitivity is given in figure AX 2. The calculation was done at a frequency of 1 Hz and for a ring with a perimeter of 360 m, with 120 inlet ports , every 3 m of 120 acoustic ohm resistance. The tube had a cross-section diameter of 50 mm. For comparison with respect to the scale of figure AX 2: the slowness of a horizontal sound wave is approximately 3 s/km. It is clear that the overall pattern is asymmetric. At wavelengths of the order of the diameter of the ring the angular dependence is strong. This is in marked contrast with a noise reducer in a star formation. At lower frequencies the pattern of angular dependence becomes more symmetrical. For applications in an array, ring shaped noise reducers should have their microbarograph detectors positioned identical, all in the same direction with respect to the midpoint of the ring. This avoids systematic timing errors.

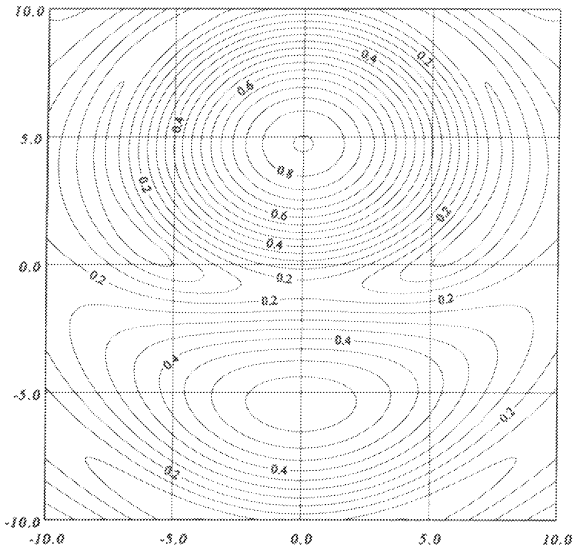

Figure AX 2.
Power of the response function of a circular noise reducer. The horizontal and vertical axes are two components of horizontal slowness in s/km.

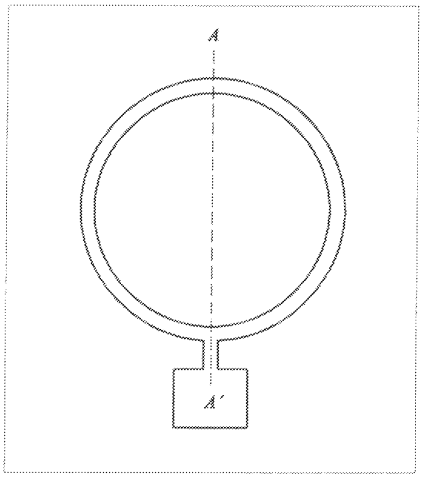

Figure AX 3.
Symmetry of a circular noise reducer.

In figure AX 3 the ring-shaped noise reducer is shown, the barometer is attached to the bottom of the ring. The axis *A* - *A´* is the axis of mirror symmetry. All the physical properties have the same symmetry, such as the pressure modes in the ring. It follows that in *A* and in *A´* there is a pressure maximum i.e. an antinode. Of course, the other solution - a pressure node at *A* and in *A´* - is also possible. This mode, however, will not produce a signal to the microbarograph; because of the symmetry no volume flux will occur at *A*. Thus the impedance in *A* is infinite. The ring-shaped noise reducer is therefore equivalent with a reducer with two branches, both terminated with a stopper.

Burridge, B., The Acoustics of Pipe Arrays, *Geophys. J. R.. astr. Soc.*, **26**, 53-69, 1971.
Rayleigh, J. W. S., The Theory of Sound, volume II, § 264, p. 63-66, Dover, 1945

References

Benade, A. H., On the Propagation of Sound Waves in a Cylindrical Conduit, *J. acoust. Soc. Am.*, **44**, 616-623, 1968.

Burridge, B., The Acoustics of Pipe Arrays, *Geophys. J. R.. astr. Soc.*, **26**, 53-69, 1971.

Carter, G. W., and A. Richardson, Techniques of circuit analysis, Cambridge, 1972.

Cook, R. K., and A. J. Bedard, Jr., On the Measurement of Infrasound, *Geophys. J. R.. astr. Soc.*, **26**, 5-11, 1971.

Daniels, F. B., On the Propagation of Sound Waves in a Cilindrical Conduit, *J. acoust. Soc. Am.*, **22**, 563-564, 1950.

Daniels, F. B., Noise-reducing line microphone for frequencies below 1 cps, *J. acoust. Soc. Am.*, **31**, 529-531, 1959.

Grover, F. H., Experimental Noise Reducers for an Active Microbarograph Array, *Geophys. J. R.. astr. Soc.*, **26**, 41-52, 1971.

Haak, H. W., An Acoustical Array for Subsonic Signals, in press, 1996.

Leonard, R. W., Simplified Flow Resistance Measurement, *J. acoust. Soc. Am.*, **17**, 240-241, 1946.

Mason, W. P., Electromechanical Transducers and Wave Filters, van Nostrand, 1958.

Moore, W. J., Physical Chemistry, 5ed., p 152-154, Longman, 1972.

Morse, P. M., and K. U. Ingard, Theoretical Acoustics, McGraw-Hill (1968).

Owen, G. W., and P. W. Keaton, Fundamentals of Electronics, Vol. I, p 254, Harper International Ed., 1966.

Ower, E., and R. C. Panchurst, The Measurement of Air Flow, Pergamon Press, 1977.

Rayleigh, J. W. S., The Theory of Sound, Dover, 1945.

Rschevkin, S. N., The theory of sound, Pergamon Press, 1963.

Shoemaker, D. P., and C. W. Garland, Experiments in Physical Chemistry, 2ed., McGraw-Hill Kogakusha, ltd., 1967.

Zwikker, C., and C. W. Kosten, Sound Absorbing Materials, Elsevier, 1949.

KNMI-Publicaties, Technische & Wetenschappelijke Rapporten gepubliceerd sedert 1988

Een overzicht van alle publicaties van het Koninklijk Nederlands Meteorologisch Instituut die tussen 1849 en 1988 werden uitgegeven, wordt u op verzoek toegezonden door de Bibliotheek van het KNMI, postbus 201, 3730 AE De Bilt, tel. 030 - 2 206 855, fax. 030 - 2 210 407.

KNMI-publicatie met nummer

150-27	Normalen en extreme waarden van 15 hoofdstations voor het tijdvak 1961-90 / samenst. H.J. Krijnen ...[et al.]	1992
165-5	Historische weerkundige waarnemingen: beschrijving antieke meetreeksen / H.A.M. Geurts en A.F.V. van Engelen	1992
172	Vliegen in weer en wind: geschiedenis van de luchtvaartmeteorologie / Tj. Langerveld	1988
173	Werkdocument verspreidingsmodellen / red. H. van Dop ; in samenwerking met het RIVM	1988
174	Ons klimaat, onze planeet / voorw. H. Tennekes ; inleiding C.J.E. Schuurmans ; met bijdr. van H. van Dop ...[et al.]	1989
175	Klimaat-onderzoek Westland ten behoeve van kustuitbreiding / W.H. Slob	1989
176	Stormenkalender: chronologisch overzicht van alle stormen langs de Nederlandse kust 1964-1990 / B. Augustijn, H. Daan ...[et al.]	1990
177	Description of the RIVM-KNMI PUFF dispersion model / G.H.L. Verver ...[et al.]	1990
178	Modules A & B / Bureau Vorming en Opleiding **[uitsluitend intern beschikbaar]**	1991-
179	Catalogus van aardbevingen in Nederland / G. Houtgast	1991
179a	Catalogus van aardbevingen in Nederland : 2e, gewijzigde druk / G. Houtgast	1992
180	List of acronyms in environmental sciences / [P. Geerders]	1991
180a	List of acronyms in environmental sciences : revised edition / [P. Geerders and M. Waterborg]	1995
181	Nationaal gebruik van de groepen 7wwW1W2 en 960ww voor landstations / [samenst. H. van Drongelen ea.]	1992
181a	FM12 Synop : internationale en nationale regelgeving voor het coderen van de groepen 7wwW1W2 en 960ww	1995
181b	FM12 Synop : internationale en nationale regelgeving voor het coderen van de groepen 7wwW1W2 en 960ww ; derde herziene versie	1996
182	Wijziging aeronautische codes : 1 juli 1993 / [P.Y. de Vries en A.A. Brouwer]	1993
183-1	Rainfall in New Guinea (Irian Jaya) / T.B. Ridder	1995
183-2	Vergelijking van zware regens te Hollandia (Nieuw Guinea), thans Jayapura (Irian Jaya) met zware regens te De Bilt / T.B. Ridder	1995
183-3	Verdamping in Nieuw-Guinea, vergelijking van gemeten hoeveelheden met berekende hoeveelheden / T.B. Ridder	1995
183-4	Beschrijving van het klimaat te Merauke, Nieuw Guinea (Irian Jaya) in verband met de eventuele vestiging van een zoutwinningsbedrijf aldaar / T.B. Ridder en H.W.H. Weeda	1995
183-5	Overzicht van klimatologische en geofysische publikaties betreffende Nieuw-Guinea / T.B. Ridder	1995
184	Inleiding tot de algemene meteorologie : studie-uitgave / B. Zwart, A. Steenhuisen, m.m.v. H.J. Krijnen	1994
184a	Inleiding tot de algemene meteorologie : studie uitgave ; 2e, geheel herziene druk / B. Zwart, A. Steenhuisen, m.m.v. H.J. Krijnen ea.	1995
185	Handleiding voor het gebruik van sectie 2 van de FM 13-X SHIP code door stations op zee / KNMI; Kon. Luchtmacht; Kon. Marine	1994
185a	Handleiding voor het gebruik van sectie 2 van de FM 13-X SHIP-code voor waarnemers op zee / KNMI; Kon.Luchtmacht, Kon.Marine	1995

Overigen

Zonnestraling in Nederland / C.A. Velds (in samenwerking met uitgeverij Thieme in de serie "Het klimaat van Nederland"; 3)	1992

Technisch rapport = technical report (TR) - ISSN 0169-1708

103a	Wind-chill [geheel herziene versie] / B. Zwart	1992
105	Description of the Cabauw turbulence dataset 1977-1979 / C. Hofman	1988
106	Automatische detektie van inversies met sodar / A.C.M. Beljaars en R. Agterberg	1988
107	Numerieke atmosfeermodellen / A.P.M. Baede	1988
108	Inpassing van Meteosat informatie in de meteorologische besluitvorming / J. Roodenburg	1988
109	Opmeting van het aardmagneetveld in Nederland, herleid naar 1985 / J.H. Rietman	1988
111	Van Penman naar Makkink: een nieuwe berekeningswijze voor de klimatologische verdampingsgetallen / red. J.C. Hooghart ...[et al.]	1988
112	Description of a software library for the calculation of surface fluxes / A.C.M. Beljaars ...[et al.]	1989
113	Menghoogteberekeningen voor het Europees continent: een vergelijkend onderzoek / M.P. Scheele en H. van Dop	1989
114	Operational WAMS statistics over the period December 1986 - March 1987 / R.A. van Moerkerken ...[et al.]	1989
115	Mesoscale terrain roughness mapping of the Netherlands / R. Agterberg and J. Wieringa	1989
116	Geschiedenis van de landbouwmeteorologie in Nederland tot 1972 / J.P.M. Woudenberg	1989
117	Instabiliteiten rond de straalstroom / R.P. Henzen	1989
118	Verfificatie van de GONO golfverwachting over de periode oktober 1987 - april 1988 / R.A. van Moerkerken	1989
119	Spectra en gradienten van hoge windsnelheden te Cabauw tot 200 meter / R.W.M. Meijer	1989
120	About the possibilities of using an air transformation model in Tayun, Shanxi province, China / J. Reiff ...[et al.]	1989
121	The effect of wave data assimilation of the numerical simulation of wave energy advection / M. de las Heras ...[et al.]	1990
122	Objective analysis of precipitation observations during the Chernobyl episode / M.P. Scheele and G.H. Verver	1990
123	The use of satellite data in the ECMWF analysis system / K. Lablancz	1990
124	A primitive equation model for the Equatorial Pacific / M.A.F. Allaart and A. Kattenberg	1990
125	Technical description of the high-resolution air mass transformation model at KNMI / E.I.F. de Bruin ...[et al.]	1990
126	Verificatie kwantitatieve neerslagverwachting korte termijn (proefperiode) voor 5 regio's / D. Messerschmidt	1990
127	Quantitative processing of Meteosat-data: implementation at KNMI: applications / S.H. Muller	1990
128	A primary experiment of statistical interpolation schemes used in sea wave data assimilation / Gao Quanduo	1990
129	Coordinate conversions for presenting and compositing weather radar data / H.R.A. Wessels	1990
130	Flux-profile relationships in the nocturnal boundary layer / P. Bouwman	1990
131	The implementation of the WAQUA/CSM-16 model for real time storm surge forecasting / J.W. de Vries	1991
132	De luchttemperatuur boven West-Ameland / F. Ynsen	1991
133	Seizoenverloop en trend in de chemische samenstelling van de neerslag te Lelystad / T.A. Buishand en J.H. Baard	1991
134	Technical description of LAM and OI: Limited Area Model and Optimum Interpolation analysis / W.C. de Rooy ...[et al.]	1991
134a	Technical description of LAM and OI: Limited Area Model and Optimum Interpolation analysis, 2nd edition / W.C. de Rooy ...[et al.]	1992
135	Relatieve trajectorien in en rond een depressie / J.P.A.J. van Beeck	1991
136	Bepaling van een directe en diffuse straling en van zonneschijnduur uit 10-minuutwaarden van de globale straling / W.H. Slob ...[et al.]	1991

137	LAM en NEDWAM statistics over the period October 1990 - April 1991 / R.A. van Moerkerken	1991
138	Dagsom van de globale straling : een rekenmethode en verwachtingsverificatie / M.C. Nolet	1991
139	A real-time wave data quality control algorithm / Maria Paula Etala	1991
140	Syllabus Fysische Meteorologie I / H.R.A. Wessels	1991
141	Systeembeschrijving Mist Voorspel Systeem MIVOS / D. Blaauboer, H.R.A. Wessels en S. Kruizinga	1992
142	Het nachtelijk windmaximum : een interactieve verwachtingsmethode / N. Maat en H. Bakker	1992
143	Neerslagverificatie LAM / W.C. de Rooy en C. Engeldal	1992
144	Aanpassing vocht-bedekkingsgraadrelaties in het LAM / W.C. de Rooy	1992
145	Een verificatie van de Eurogids, de gidsverwachting voor vervoer en toerisme / H.G. Theihzen	1992
146	The earth radiation budget experiment : overview of data-processing and error sources / Arnout J. Feijt	1992
147	On the construction of a regional atmospheric climate model / Jens H. Christensen and Erik van Meijgaard	1992
148	Analyse van torenwindgegevens over het tijdvak 1977 tot en met 1991 / Gertie Geertsema	1992
149	The performance of drag relations in the WAQUA storm surge model / J.R.N. Onvlee	1993
150	Verifications of 3I retrievals vis-à-vis radiosonde observations / G.J. Prangsma	1993
151	Het Synoptisch Symposium : een verslag / red. H.G. Theihzen	1993
152	The ACIFORN hydrological programme : the water cycle of a Douglas fir forest / F.C. Bosveld ...[et al.]	1993
153	Het APL+-prgramma / R.M. van Westrhenen	1993
154	The effect of spatial averaing on threshold exceedances of daily precipitation amounts / T.A. Buishand,	1993
155	Neerslagvergelijking van Espelo ten opzichte van het omgevingsgemiddelde / J.P.M. van Dun en J. Verloop	1993
156	On the effects of limited spectral resolution in third-generation wave models / I.V. Lavrenov and J.R.A. Onvlee	1993
157	Meteorologische evaluatie van de zichtmetingen langs de A16 / H.R.A. Wessels	1993
158	Het programma voor berekening van zonneschijnduur uit globale straling / U. Bergman	1993
159	Verificatie weersverwachtingen 1955 - 1993 / H. Daan	1993
160	Drie objectieve indices voor clear-air turbulence nader bekeken / H. Bakker	1993
161	The ASGASEX experiment / W.A. Oost	1994
162	TEBEX observations of clouds and radiation -potential and limitations / P. Stammes ...[et al.]	1994
163	Evaluatie kwaliteitsonderzoek mistdata "Mistprojekt A-16" Breda / M. van Berchum	1994
164	Standaard stralingsmetingen met een zonnevolger / A.C.A.P. van Lammeren en A. Hulshof	1994
165	Neurale netwerken versus lineaire regressie / R.M. Meuleman	1994
166	Seismische analyse van de aardbeving bij Alkmaar op 6 augustus 1994 / [SO]	1994
167	Seismische analyse van de aardbeving bij Alkmaar op 21 september 1994 / [SO]	1994
168	Analyse van het seismische risico in Noord-Nederland / Th. de Crook, B. Dost en H.W. Haak	1995
169	Evaluatie van neerslagprognoses van numerieke modellen voor de Belgische Ardennen in december 1993 / Erik van Meijgaard	1994
170	DARR-94 / C.P.G. Lomme	1994
171	EFEDA-91 : documentation of measurements obtained by KNMI / W.A.A. Monna ...[et al.]	1994
172	Cloud lidar research at the Royal Netherlands Meteorological Institute and KNMI2B2 version 2 cloud lidar analysis software documentation / Alexandre Y. Fong and André C.A.P. van Lammeren	1994
173	Measurements of the structure parameter of vertical wind-velocity in the atmospheric boundary layer / R. van der Ploeg	1995
174	Report of the ASGASEX'94 workshop / ed. by W.A. Oost	1995
175	Over slecht zicht, bewolking, windstoten en gladheid / J. Terpstra	1995
176	Verification of the WAQUA/CSM-16 model for the winters 1992-93 and 1993-94 / J.W. de Vries	1995
177	Nauwkeuriger nettostraling meten / M.K. van der Molen en W. Kohsiek	1995
178	Neerslag in het stroomgebied van de Maas in januari 1995: waarnemingen en verificatie van modelprognoses / Rudmer Jilderda ...[et al.]	1995
179	First field experience with 600PA phased array sodar / Henk Klein Baltink	1995
180	Een Kalman-correctieschema voor de wegdektemperatuurverwachtingen van het VAISALA-model / A. Jacobs	1995
181	Calibration study of the K-Gill propeller vane / Marcel Bottema	1995
182	Ontwikkeling van een spectraal UV-meetinstrument / Frank Helderman	1995
183	Rainfall generator for the Rhine catchment : a feasibility study / T. Adri Buishand and Th o Brandsma	1996
184	Parametrisatie van mooi-weer cumulus / M.C. van Zanten	1995
185	Interim report on the KNMI contributions to the second phase of the AERO-project / Wiel Wauben, Paul Fortuin ...[et al.]	1995
186	Seismische analyse van de aardbevingen bij Middelstum (30 juli 1994) en Annen (16 augustus 1994 en 31 januari 1995) / [SO]	1995
187	Analyse wenselijkheid overname RIVM-windmeetlokaties door KNMI / H. Benschop	1996
188	Windsnelheidsmetingen op zeestations en kus stations: herleiding waarden windsnelheden naar 10-meter niveau / H. Benschop	1996
189	On the KNMI calibration of net radiometers / W. Kohsiek	1996
190	NEDWAM statistics over the period October 1994 - April 1995 / F.B. Koek	1996
191	Description and verification of the HIRLAM trajectory model / E.I.F. de Bruijn	1996
192	Tiltmeting : een alternatief voor waterpassing ? / H.W. Haak	1996
193	Error modelling of scatterometer, i-situ and ECMWF model winds; a calibration refinement / Ad Stoffelen	1996

Wetenschappelijk rapport = scientific report (WR) - ISSN 0169-1651

88-01	Central Sudan surface wind data and climate characteristics / E.H. ABu Bakr
88-02	Startocumulus modeling / P.G. Duynkerke
88-03	Naar een niet-linear wateropzetmodel : stand van zaken februari 1988 / C.J. Kok
88-04	The boundary layer wind regime of a representative tropical African region, central Sudan / E.H. ABu Bakr
88-05	Radiative cooling in the nocturnal boundary layer / S.A. Tjemkes
88-06	Surface flux parameterization schemes : developments and experiences at KNMI / A.A.M. Holtslag and A.C.M. Beljaars
89-01	Instability mechanisms in a barotropic atmsophere / R.J. Haarsma
89-02	Climatological data for the North Sea based on observations by volutary observing ships over the period 1961-1980 / C.G. Korevaar
89-03	Verificatie van GONO golfverwachtingen en van Engelse fine-mesh winden over de periode oktober 1986 - april 1987 / R.A. van Moerkerken
89-04	Diagnostics derivation of boundary layer parameters from the outputs of atmospheric models / A.A.M. Holtslag ...[et al.]
89-05	Statistical forecasts of sushine duration / Li Zhihong and S. Kruizinga
90-01	The effect of a doubling atmospheric CO2 on the stormtracks in the climate of a GCM / P.C. Siegmund
90-02	Analysis of regional differences of forecasts with the multi-layer AMT-model in the Netherlands / E.I.F. de Bruin, Li Tao Guang ...[et al.]
90-03	Description of the CRAU- data-set: Meteosat data, radiosonde data, sea surface temperatures : comparison of Meteosat and Heimann-data / S.H. Muller, H. The, W. Kohsiek and W.A.A. Monna
90-04	A guide to the NEDWAM wave model / G. Burgers
91-01	A parametrization of the convective atmospheric boundary layer and its application into a global climate model / A.A.M. Holtslag ...[et al.]

91-02 Turbulent exchange coefficients over a Douglas fir forest / F.C. Bosveld
92-01 Experimental evaluation of an arrival time difference lightning positioning system / H.R.A. Wessels
92-02 GCM control run of UK Met.Office compared with the real climate in the Northwest European winter / J.J. Beersma
92-03 The parameterization of vertical turbulent mixing processes in a General Circulation Model of the Tropical Pacific / G. Janssen
92-04 A scintilation experiment over a forest / W. Kohsiek
92-05 Grondtemperaturen / P.C.T. van der Hoeven en W.N. Lablans
92-06 Automatic supression of anomalous propagation clutter for noncoherent weather radars / H.R.A. Wessels ...[et al.]
93-01 Searching for stationary stable solutions of Euler's equation / R. Salden
93-02 Modelling daily precipitation as a function of temperature for climatic change impact studies / A.M.G. Klein Tank and T.A. Buishand
93-03 An analytical conceptual model of extratropical cyclones / L.C. Heijboer
93-04 A synoptic climatology of convective weather in the Netherlands / Dong Hongnian
93-05 Conceptual models of severe convective weather in the Netherlands / Dong Hongnian
94-01 Seismische analyse van aardbevingen in Noord-Nederland : bijdrage aan het multidisciplinaire onderzoek naar de relatie tussen gaswinning en aardbevingen / H.W. Haak en Th. de Crook
94-02 Storm activity over the North Sea and the Netherlands in two climate models compared with observations / J.J. Beersma
94-03 Atmospheric effects of high-flying subsonic aircraft / W. Fransen
94-04 Cloud-radiation-hydrological interactions : measuring and modeling / A. Feijt ...[et al.]
94-05 Spectral ultraviolet radiation measurements and correlation with atmospheric parameters / F. Kuik and H. Kelder
95-01 Transformation of precipitation time series for climate change impact studies / A.M.G. Klein Tank and T.A. Buishand
95-02 Internal variability of the ocean generated by a stochastic forcing / M.H.B. van Noordenburg
95-03 Applicability of weakly nonlinear theory for the planetary-scale flow / E.A. Kartashova
95-04 Changes in tropospheric NOx and O3 due to subsonic aircraft emissions / W.M.F. Wauben ...[et al.]
95-05 Numerical studies on the Lorenz-84 atmosphere model / Leonardo Anastassiades
95-06 Regionalisation of meteorological parameters / W.C. de Rooy
95-07 Validation of the surface parametrization of HIRLAM using surface-based measurements and remote sensing data / A.F. Moene, H.A.R. de Bruin ...[et al.]
95-08 Probabilities of climatic change : a pilot study / Wieger Fransen (ed.) and Alice Reuvekamp
96-01 A new algorithm for total ozone retrieval from direct sun measurements with a filter instrument / W.M.F. Wauben
96-02 Chaos and coupling: a coupled atmosphere ocean-boxmodel for coupled behaviour studies / G. Zondervan
96-03 An acoustical array for subsonic signals / H.W. Haak
96-04 Transformation of wind in the coastal zone / V.N. Kudryavtsev and V.K. Makin
96-05 Simulations of the response of the ocean waves in the North Atlantic and North Sea to CO2 doubling in the atmosphere / Kathy M. Rider ...[et al.]
96-06 Microbarograph systems for the infrasonic detection of nuclear explosions / H.W. Haak and G.J. de Wilde